Université Mohamed Khider de Biskra
Faculté des Sciences et de la Technologie
Département de génie électrique

MÉMOIRE DE MASTER

Sciences et Technologies
Field: Electrical Engineering
Specialization: Electric Control

Réf. : Entrez la référence du document

Présenté et soutenu par :
ZAHGEZ AMINA

Le : mercredi 4 juin 2025

Direct Torque Control of The Induction Machine:Theoretical and Experimental study

---

Jury :

Pr	Abdeddaim Sabrina	Professor	University of Biskra	President
Pr	Sraiei Kamel	Professor	University of Biskra	Examiner
Pr	Benchouia Mohamed Toufik	Professor	University of Biskra	Reviewer

Année universitaire : Choisissez une année

Université Mohamed Khider de Biskra
Faculté des Sciences et de la Technologie
Département de génie électrique

MÉMOIRE DE MASTER

Sciences et Technologies
Field: Electrical Engineering

Electric Control

Réf. : Entrez la référence du document

Direct Torque Control of The Induction Machine:Theoretical and Experimental study

Le : ……

Présenté par :

Avis favorable de l'encadreur :

Signature Avis favorable du Président du Jury

Cachet et signature

Acknowledgments

I would like to express my sincere gratitude to ALLah and all those who contributed, directly or indirectly, to the completion of this work.

First and foremost, I warmly thank my supervisor, ***Pr. Benchouia Mohamed Toufik*** *, for their availability, valuable guidance, and support throughout this project. Their expertise and constant encouragement have been invaluable , I also wish to thank doctoral student* ***Fares bettaher*** *and* ***Fella boucetta*** *They did everything they could and I appreciate them for that.*

I would also like to thank Professor ***Naimie jemai****, professor at the University of Biskra and Director of the Electrical Engineering Laboratory of Biskra (LGEB).*

I also thank all the teachers at the Electrical Engineering Department of the University of Biskra.

إهداء:

يا من إذا ضاقت بي السُبلُ وسَعَت، وإذا خَفَت الأمل أضاء
يا واهب العقل بيانًا، والقلبَ سكينةً، والروحَ صبرًا على عناء الدرب
لك الحمدُ ما نبض قلبٌ بالحياة، وما ارتفع في الدجى دعاء
لك السجود شكرًا، ولك الثناء مدًى، فما أنا إلا بفيض جودك
إلى من سهرت الليالي من أجلي، إلى من تخلّت عن راحتها لتصنع راحتي،
إلى من كانت تهمس بدعائها كلّما شعرتُ بالضعف
إلى أمي الأستاذة " **رزيقة دكالي**" ، يا وطنًا لا يغيب، ويا دفئًا لا يبرد، يا نبض قلبي وسبب نجاحي
هذا الإنجاز لكِ، يا أغلى ما أملك، وكم تمنيتُ لو أستطيع أن أزرع في كل صفحة من هذه المذكرة قبلة عرفان على جبينك الطاهر.
إلى أبي العزيز الغالي الّذي أحمل إسمه بكل إفتخار "**زاغز توفيق**"و جدتي الحبيبة و الحنونة "**فضيلة زاغز**"و "**بالنولي ام هاني**"
لأخوّة ليست حروفًا تُنطق، بل أرواحٌ تتآلف، وقلوبٌ إذا ضاقت الدنيا اتّسعت بحبّها أخي "**سراج "أدم"**و"**صلاح**"
إلى أختي الوحيدة "**سارة زاغز**" أنشودة القلب إذا خنقته الحياة
ويا ظلّ الروح إذا اشتدّ وهج الألم
أنتِ حضن لم تخلقه الأمهات، بل نسجه الله من نور الرحمة ورباط الدم
إلى "**هالة حاج لكحل**"من كنتِ لي أكثر من أخت، وأقرب من نبض القلب
كنتِ النور في عتمتي، واليد التي امتدت إليّ حينما كادت يداي تفلتان.
إلى "**سميرة**" عرفتكِ فازدادت الحياة بصحبتك، وصارت الأيام أرحم لأنكِ فيها ،أنتِ الحضور الجميل في كل لحظة، والصوت الذي يربّت على قلبي دون أن ينطق.
إلى "**يتوجي بيسان**" قد كانت رفيقتي في العمل مثالًا يُحتذى به في اللباقة والروح الطيبة ، تقاسمنا ضغوط العمل بلطفٍ وتفهم، ولن أنسى أبدًا كلماتها المشجعة ومواقفها النبيلة، التي تركت في نفسي أثرًا عميقًا من الامتنان.

Chapter 1 : Modeling of the Induction Machine

Chapter II Control Techniques for Induction Machine

Chapter 03: Direct Torque Control of an Induction Machine

Chapter 4 : Experimental validation.

Notation and symbols

S_a, S_b and S_c: the magnetic axes of the stator phases.
R_a, R_b and R_c: the magnetic axes of the rotor phases.
$[V_{sabc}]\ et\ [V_{rabc}]$: Stator and rotor voltage vectors respectively.
$[i_{sabc}]\ et\ [i_{rabc}]$: Stator and rotor current vectors respectively.
$[\Psi_{sabc}]\ et\ [\Psi_{rabc}]$: Stator and rotor flux vectors respectively.
$[R_s]\ et\ [R_r]$: The stator and rotor resistance matrices respectively
$[L_s]\ et\ [L_r]$: Are the stator and rotor inductance matrices respectively.
$[M_{sr}]$: The mutual inductance matrix that corresponds to the effect of the rotor on the stator.
$[M_{rs}]$: The mutual inductance matrix that corresponds to the effect of the stator on the rotor.
L_1: The stator self-inductance.
M_1: Mutual inductance between the stator phases.
L_2: Rotor self-inductance.
M_2: Mutual inductance between the rotor phases.
$Ls = L1 - M1$: Stator cyclic inductance.
$Lr = L2 - M2$: Rotor cyclic inductance.
$L_m = 3/2\ M_{max}$: Cyclic mutual inductance between the stator and the rotor.
M_{max}: Maximum mutual inductance between the stator and the rotor when their axes coincide.
T_{em}: The electromagnetic torque of the machine.
T_r: The resistive torque of the mechanical load.
J: The moment of inertia.
f: The coefficient of friction.
Ω: The mechanical rotational speed.
Ω_n: The nominal mechanical rotational speed. Ωs: The synchronous speed.
g: Slip
[Tαβ]: Concordia transformation matrix.
ω_e: The electrical rotational speed of the rotor.
ω_s: Stator pulsation.
ω_g: Slip pulsation.
V_s: Stator voltage.
R_s: The stator resistance.
R_r: The rotor resistance.
R_r': rotor resistance brought back to the primary.
n_p: even number of the pole.
$Temax$: Max. electromagnetic torque.
$\omega coor$: the electrical rotation speed of the two-phase system U, V relative to the stator.
a, b, c: The indices of the axes of the three-phase system.
U, V,O: The indices of the axes of the two-phase system.
α, β: the indices of the axes corresponding to the reference frame linked to the stator.
d, q: the indices of the axes corresponding to the reference frame linked to the rotating field.
X, Y: the indices of the axes corresponding to the rotor reference frame.

V_1, V_2, V_3: the voltages of the three-phase network system.
U_{red}: the instantaneous voltage at the rectifier output.
V_{max}: Maximum value of the network voltage.
U_f: the voltage at the filter output.
L: The filter current smoothing inductance.
C: The filter voltage smoothing capacitor.
f: frequency.
Si: the three arms of the inverter or "i=1, 2, 3".
P: Laplace operator.
τ: The time constant. τr: Rotor time constant. σ: the dispersion coefficient.
$[X]$: The state vector.
$[A]$: State matrix.
$[U]$: The input or control vector.
$[B]$: Input or control matrix.
$\| \overline{\Psi_s} \|$: modulus of the stator flux vector.
$\| \overline{\Psi_r} \|$: modulus of the rotor flux vector.
δ: angle between the stator and rotor flux vectors.
Te: sampling time.
$\overline{\Psi_{s0}}$: is the initial stator flux vector.
$\overline{\Psi_s}$: the stator flux vector.
$V_{s\alpha}$: Stator voltage in α coordinate.
$V_{s\beta}$: Stator voltage in β coordinate.
isβ: Stator flux in β coordinate.
Vdc: DC voltage.
Δ: The sector in which the vector $\overline{\overline{F}}\boldsymbol{s}$ lies.
$\Psi_{s\,ref}$: The stator flux reference value.
$\Delta\Psi_s$: The hysteresis band width of the stator flux corrector.
Cflx: Represents the output state of the stator flux comparator.
$T_{em\ ref}$: The electromagnetic torque reference value.
FOC: Field Oriented Control.
DTC: Direct Torque Control.
IM: induction Machine.
PMSM: Permanent magnet, synchronous motor.
PWM: Pulse Width Modulation.
Other symbols used are defined in the text.

List of Tables and Figures

Chaptre 02

Chapter 03

Chapter 04

Résumé-Abstract- ملخص

Abstract:

The induction motor has become increasingly prominent in variable speed drive applications due to its robustness, low processing cost, and simple construction. In this study, we focused on the Direct Torque Control (DTC) method for controlling induction motors. Originally proposed by Takahashi in 1985 as an alternative to the Field-Oriented Control (FOC) strategy, DTC offers a direct approach to controlling torque and flux without requiring complex transformations or current regulators. While FOC provides excellent dynamic and steady-state performance, it is sensitive to parameter variations caused by temperature changes and magnetic saturation. This drawback has driven researchers to explore more robust alternatives like DTC.

In our comparison between DTC using 6 sectors and DTC with 12 sectors, simulation results clearly showed that increasing the number of sectors significantly reduces torque and flux ripples. The 12 sector DTC provides improved dynamic response and better stability, especially under load variations, compared to the traditional 6 sector approach.

Résumé:

Le moteur asynchrone est devenu de plus en plus utilisé dans les applications à vitesse variable en raison de sa robustesse, de son faible coût de traitement et de sa construction simple. Dans cette étude, nous nous sommes concentrés sur la méthode de Commande Directe du Couple (DTC) pour le contrôle des moteurs asynchrones. Proposée initialement par Takahashi en 1985 comme alternative à la stratégie de Commande Vectorielle (FOC), la DTC offre une approche directe du contrôle du couple et du flux sans nécessiter de transformations complexes ni de régulateurs de courant. Bien que la FOC offre d'excellentes performances dynamiques et en régime permanent, elle reste sensible aux variations de paramètres causées par les changements de température et la saturation magnétique. Cette limitation a conduit les chercheurs à explorer des alternatives plus robustes, telles que la DTC.

Dans notre comparaison entre la DTC à 6 secteurs et celle à 12 secteurs, les résultats de simulation ont clairement montré que l'augmentation du nombre de secteurs réduit significativement les ondulations du couple et du flux. La DTC à 12 secteurs présente une meilleure réponse dynamique et une stabilité accrue, notamment en présence de variations de charge, comparée à l'approche traditionnelle à 6 secteurs.

ملخص:

أصبح المحرك غير المتزامن يحتل مكانة متزايدة في تطبيقات القيادة ذات السرعة المتغيرة، وذلك بفضل متانته، وانخفاض تكلفته، وبنيته البسيطة. في هذا العمل، ركزنا على تقنية التحكم المباشر في العزم للتحكم في المحركات غير المتزامنة. تم اقتراح هذه الإستراتيجية لأول مرة سنة ١٩٨٥ كبديل لطريقة التحكم المتجهية بتوجيه التدفق. توفر هذه التقنية تحكمًا مباشرًا في العزم والتدفق دون الحاجة إلى تحويلات رياضية معقدة أو منظمات للتيار. وعلى الرغم من أن الطريقة المتجهية تقدم أداءً عاليًا من حيث الاستجابة الديناميكية والثبات، إلا أنها تتأثر بتغيرات معلمات المحرك الناتجة عن تغير درجات الحرارة أو تشبع الدوائر المغناطيسية، وهو ما دفع الباحثين للبحث عن حلول أكثر موثوقية مثل التحكم المباشر.

في المقارنة بين التحكم باستخدام ٦ قطاعات والتحكم باستخدام ١٢ قطاعًا، أظهرت نتائج المحاكاة بوضوح أن زيادة عدد القطاعات تساهم في تقليل تموجات العزم والتدفق بشكل كبير. كما أن التحكم بـ١٢ قطاعًا يوفر استجابة ديناميكية أفضل واستقرارًا أكبر، خاصة في ظروف تغير الحمل، مقارنةً بالتحكم التقليدي بـ٦

General introduction

General introduction

Today, AC machines have largely replaced DC machines in industry due to their reliability and low maintenance. Induction motors, especially squirrel cage types, are widely used for their cost-effectiveness and durability in various applications, including EVs and industrial drives [1].

In the early stages of their use, induction motors were directly connected to the grid, operating at a fixed frequency and speed. However, with the advancement of modern semiconductor technology and power electronic converters, these machines have evolved to support variable frequency and speed operation. This is achieved by powering them through converters such as the voltage source inverter (VSI) [1].

For basic applications, using a variable speed motor drive in open-loop control can deliver satisfactory steady state performance without the need for speed regulation. However, in applications that demand fast dynamic response and precise speed control, open-loop control becomes inadequate. In such cases, closed-loop operation of the motor is essential. Various control techniques have been developed for this purpose and are generally categorized into scalar control and vector control methods

Scalar control, also known as the volts per hertz (V/f) method, is a straightforward approach for controlling the speed of induction motors. It maintains a constant ratio of voltage to frequency using the motor's steady-state equivalent circuit. Despite its simplicity, this method is unsuitable for high-performance applications due to its slow dynamic response and the coupling between torque and flux.

To address these limitations, vector control also referred to as field-oriented control (FOC) was introduced in the 1970s by Hasse and Blaschke. This technique enables independent control of torque and flux, similar to a separately excited DC motor. By representing motor quantities in a rotating reference frame, vector control facilitates effective operation under both steady-state and dynamic conditions, offering improved transient performance, In FOC, the transformation to the synchronous reference frame converts all motor variables into DC quantities, simplifying control. However, FOC has its drawbacks: it requires coordinate transformations that depend on the rotor flux angle, which cannot be directly measured. Additionally, the control performance is sensitive to variations in machine parameters such as stator and rotor resistance.

Direct Torque Control (DTC) for induction machines was introduced in the mid 1980s by Takahashi and Depenbrock. Compared to vector control, DTC is less sensitive to variations in machine parameters, and its control strategy is simpler due to the elimination of pulse-width modulation (PWM), current controllers, and Park transformations. Additionally, it does not rely on PI controllers, which can enhance dynamic performance and avoid issues associated with PI saturation. DTC enables efficient motor operation and delivers fast and precise torque control. Its concept is based on the direct selection of switching states for the voltage inverter connected to the motor. This selection is determined using a switching table in combination with two hysteresis controllers, which are responsible for regulating the stator flux (φ_s) and the electromagnetic torque[1].

The distinction between 12 sector and 6 sector Direct Torque Control (DTC) lies in the way they manage stator flux and torque, which affects both performance and efficiency.

In 12 sector DTC, the electrical angle is divided into 12 segments, enabling finer and more accurate control of the motor. This typically leads to smoother operation and improved performance, particularly at low speeds or during sudden load changes, Conversely, 6 sector DTC uses only six segments, making it simpler and less demanding in terms of computation. However, it may lack the precision offered by the 12 sector configuration.

Overall, the 12 sector technique tends to deliver superior results, especially when it comes to reducing torque ripple and enhancing dynamic performance in high-precision applications.

The purpose of this thesis is to highlight the main control techniques, with a particular focus on Direct Torque Control (DTC) applied to Squirrel Cage induction machine, with Comparison between two methods the classical (DTC) of 6 sector and the Improved 12 sector.

It focuses on studying Direct Torque Control (DTC) of an induction machine supplied by a two level inverter, aiming to make the system's response robust against parameter variations.

- It is essential to provide a general overview of the three-phase asynchronous machine, covering its structure, operating principle, characteristics particularly speed variation, among other aspects and modeling the asynchronous machine for control purposes, using state space formalism, followed by the presentation of the corresponding models. This forms the subject of the first chapter

- In the second chapter we will se the different control type that we applied in the induction machine like (voltage and current scalar control, also the direct and indirect vector control) with their diagrams and the direct torque control.
- in the third chapter, we explore the control technique of the asynchronous machine by presenting an overview direct torque control (DTC). The focus will then shift to a more detailed study of the latter DTC and concludes with a simulation using MATLAB/SIMULINK to validate the control algorithm. Of course, the main results obtained are also presented in this chapter.
- The final chapter is dedicated to the practical implementation of the proposed control strategies. It includes experimental validation using a three phase asynchronous motor and highlights the comparison between conventional and improved control techniques of direct torque through real time results.

We will conclude this work with a general summary that outlines all the results obtained and suggests possible future research directions to build upon the work carried out.

Chapter One:
Modeling of the Induction Machine

1.1 Introduction:

Induction machines, often referred to as asynchronous machines, represent a crucial category of rotating electric machines that operate based on Faraday's Law of electromagnetic induction hence the name "induction" machines, which reflects their underlying working principle.

These machines are powered by an alternating current (AC) supply, which is applied exclusively to the stator. This is in contrast to synchronous machines, which require AC for the stator and direct current (DC) for the rotor. Because the induction machine operates with an AC supply to the stator alone, it is classified as a singly excited machine.

Like other rotating electric machines, induction machines have a reversible mode of operation, allowing them to function both as motors and as generators. Among these applications, their use as motors is the most widespread in industry, due to several advantages: compatibility with standard AC power sources, simple and rugged construction, ease of maintenance, and reliable speed regulation [2].

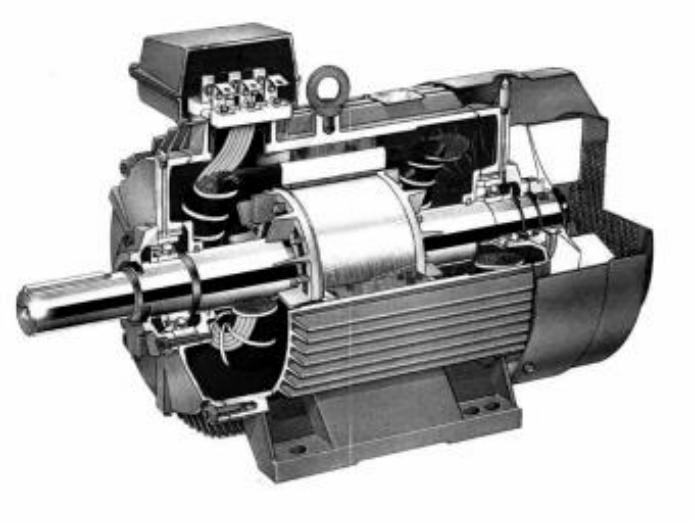

Fig(1.1): A state of the art three-phase induction motor.

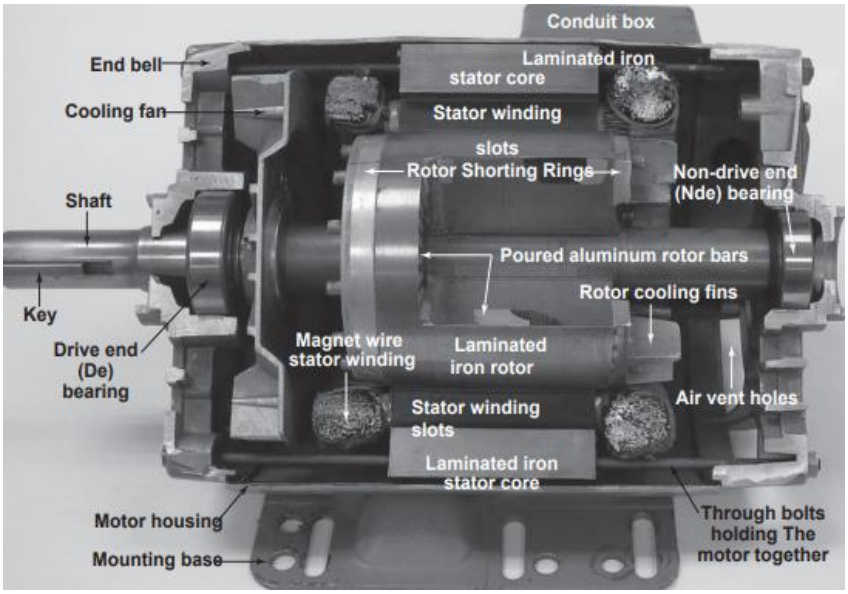

Fig (I.2) Induction motor cutaway view with labels.

1.2 Classification of Motors:

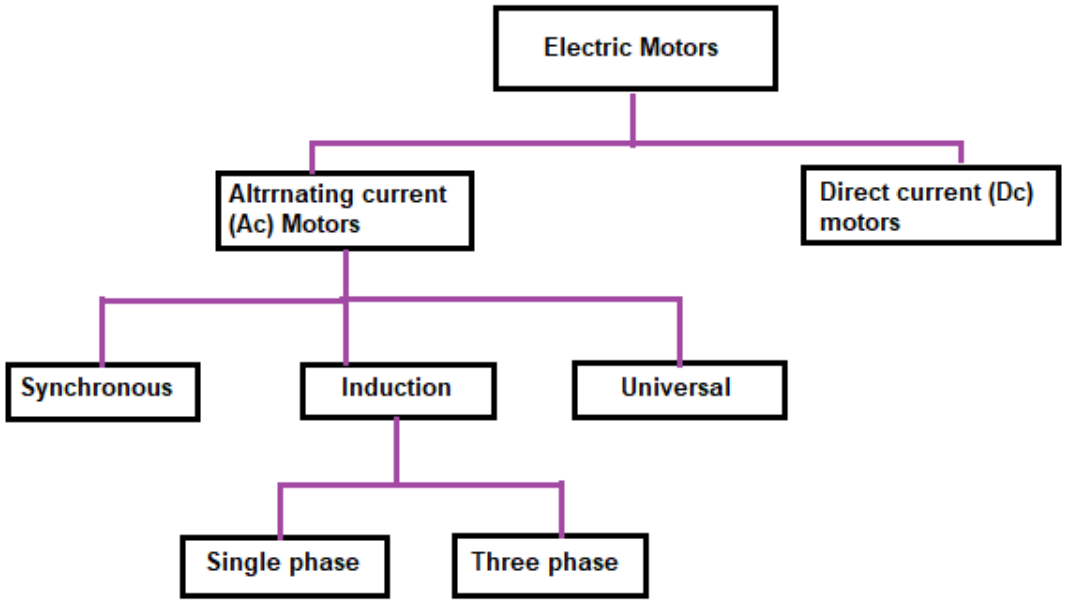

1.3 Types of the Induction Motor:

Among the various types of electric motors, squirrel cage and wound rotor motors are commonly used. Each type has unique design features and characteristics that make them well suited for particular applications [4].

1.3.1 Squirrel Cage Rotor:

The squirrel cage rotor is commonly found in both single-phase and three-phase induction motors. Its name comes from its structure, which resembles a rotating cage formed by conductive bars typically aluminum or copper embedded in a laminated cylindrical core.

These bars are short circuited at both ends with end rings, When AC power is supplied to the stator, it creates a rotating magnetic field. This field induces current in the rotor bars through electromagnetic induction, generating torque and causing the rotor to spin.

This type of rotor is popular due to its simple and durable design, high starting torque, good efficiency, and the fact that it doesn't require external electrical connections to the rotor. [4]

1.3.2 Wound Rotor :

The wound rotor also called a slip ring or phase-wound rotor is used in both single-phase and three-phase induction motors. It features windings on the rotor similar to those on the stator. These windings are connected to slip rings mounted on the rotor shaft and electrically isolated from it Carbon brushes maintain contact with the slip rings, allowing external resistors to be connected to the rotor circuit. Adjusting this resistance enables control over the motor's torque and speed. Wound rotor motors are ideal for applications requiring adjustable speed and high starting torque, such as cranes and hoists. However, they are more complex and need regular maintenance due to the slip rings and brushes[4].

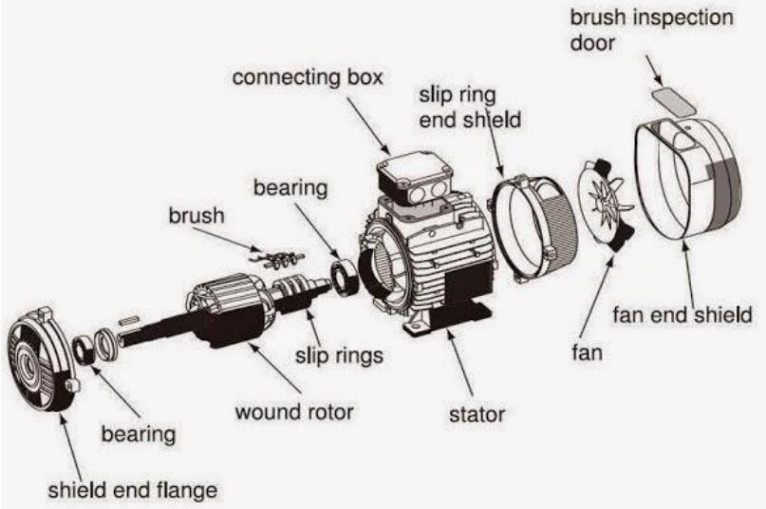

Fig (1.3). Wound rotor in induction machine.

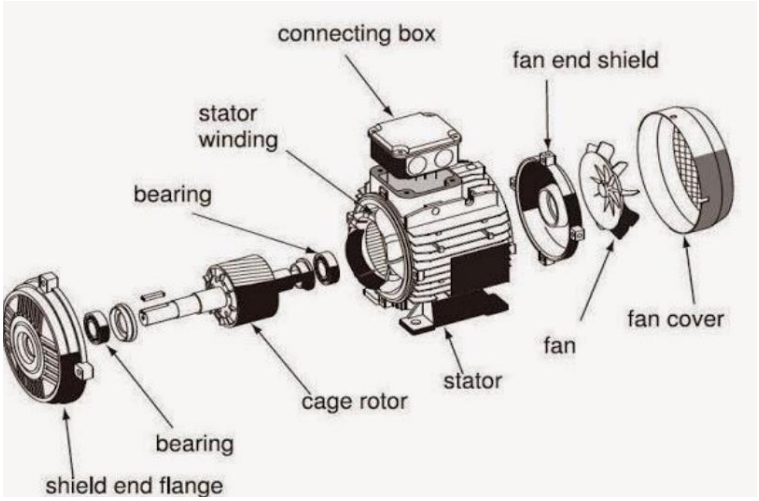

Fig (1.4). Squirrel cage rotor in induction machine [3]

1.4 Advantages and Disadvantages of Types in the Induction Motor:

	Advantages	**Disadvantages:**
Squirrel Cage Motor	• Simple construction, leading to lower cost and maintenance requirements. • High efficiency and reliability. • Suitable for applications with constant speed requirements.	• Limited speed control capabilities. • Less suitable for applications requiring variable speed operation.
Wound Rotor Motor	• High starting torque, making them suitable for applications with high starting loads. • Adjustable speed-torque characteristics. • Lower starting current compared to squirrel cage motors.	• Higher initial cost due to the complexity of the rotor windings and slip ring assembly. • Higher maintenance requirements due to the use of slip rings and brushes.

1.5 Principle of Operation:

When a three-phase AC supply is applied to the stator windings of a wound rotor induction motor, it generates a rotating magnetic field within the stator core. This field rotates at a constant angular velocity known as synchronous speed, calculated by:

$$ns = \frac{120\ f}{np} \qquad (1.1)$$

Where f is the supply frequency and np is the number of stator poles.

As the rotating magnetic field sweeps past the stationary conductors in the rotor, it induces an electromotive force (emf) in them. Because the rotor conductors are short circuited, this emf causes a current to flow. That current creates its own magnetic field, which tries to align with the rotating field of the stator. This interaction generates torque, making the rotor turn in the same direction as the stator's field[6].

However, the rotor never quite catches up to synchronous speed. If it did, there would be no relative motion between the stator field and the rotor, meaning no emf would be induced no current, and therefore, no torque. That's why an induction motor always runs just a little slower than synchronous speed[6].

1.6 Modeling of the Induction Machine:

To effectively control electric motors, it's essential not only to understand their behavior but also to develop accurate theoretical models that reflect their real-world performance. Electrical engineers aim to create detailed models that represent the machine's response in both steady state and dynamic conditions, especially considering that motor design must account for transient phases such as start up or load changes which are often more demanding than steady operation. Therefore, these models must be suitable for analyzing the motor's performance under all operating conditions [6].

1.7 Presentation of an Asynchronous Machine:

The asynchronous machine has three stator windings supplied by a three-phase current system and three rotor windings short-circuited on themselves crossed by a three-phase current system. The axes of each winding system are offset by 120 degrees.

θr is the electrical (or mechanical) angle between the axis of the stator phase (A) and the rotor phase (a)[6].

The three-phase asynchronous machine can be considered as represented by the windings in the figure:

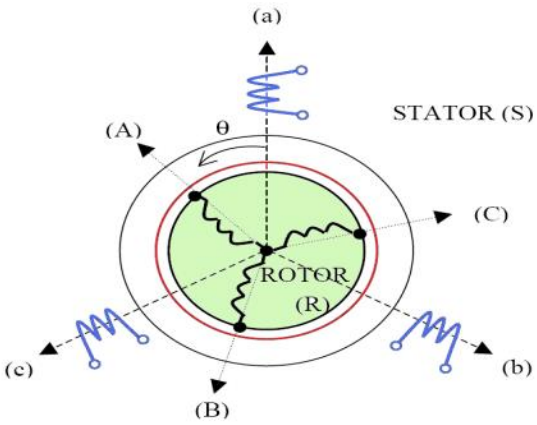

Fig(1.5): Vector Representation of the Windings of the Asynchronous Machine.

1.8 Simplifying assumptions:

For the equations of the asynchronous machine, we assume that:

- The winding is distributed so as to give a sinusoidal m.f.m. if it is supplied by sinusoidal currents.
- The magnetic circuit is not saturated.
- The air gap is constant.
- The iron losses are negligible.

Among the meanings of these hypotheses we can cite:

- The fluxes are additive.
- The self-inductances are constant.
- There is a sinusoidal variation of the mutual inductances between the stator and rotor windings as a function of the electrical angle of their magnetic axes [6].

1.9 Equations of the induction machine:

a.Electrical Equations:

The voltage equations that describe the 3 circuits are:

$$U_{as} = R_s \, \mathrm{I}_{as} + \frac{\mathrm{d}\Psi_{as}}{\mathrm{dt}} \qquad (1.2)$$

$$U_{ar} = R_r \, \mathrm{I}_{ar} + \frac{\mathrm{d}\Psi_{ar}}{\mathrm{dt}} \qquad (1.3)$$

$$U_{bs} = R_s \, I_{bs} + \frac{d\Psi_{bs}}{dt} \quad (1.4)$$

$$U_{br} = R_r \, I_{br} + \frac{d\Psi_{br}}{dt} \quad (1.5)$$

$$U_{cs} = R_s \, I_{cs} + \frac{d\Psi_{cs}}{dt} \quad (1.6)$$

$$U_{cr} = R_r \, I_{cr} + \frac{d\Psi_{cr}}{dt} \quad (1.7)$$

U_{as} U_{bs} U_{cs}: Voltages in the three stator phases

$\mathbf{I}_{as}$, $\mathbf{i}_{bs}$, $\mathbf{i}_{cs}$: Currents in the three stator phases

Ψ_{as}, Ψ_{bs} Ψ_{cs} : Total flux through these windings

U_{ar} U_{br} U_{cr}: rotor Voltages

$\mathbf{I}_{ar}$, $\mathbf{i}_{br}$, $\mathbf{i}_{cr}$:rotor Currents

Ψ_{ar}, Ψ_{br} Ψ_{cr} : Rotor fluxes

R_s: Resistance of a stator phase

$R_{r:}$ Resistance of a rotor phase

The 1st and the second equations in a matrix form, become:

$$[U_{abcs}] = [R_s][I_{abcs}] + \frac{d[\Psi_{abcs}]}{dt} \quad (1.8)$$

$$[U_{abcr}] = [R_r][I_{abcr}] + \frac{d[\Psi_{abcr}]}{dt} \quad (1.9)$$

b.Magnetic Equations:

The fluxes coupled with the stator and rotor phases with the form:

For the stator:

$$\begin{bmatrix}\Psi_{as}\\ \Psi_{bs}\\ \Psi_{cs}\end{bmatrix} = [L_s] \begin{bmatrix}i_{as}\\ i_{bs}\\ i_{cs}\end{bmatrix} + [Msr] \begin{bmatrix}i_{ar}\\ i_{br}\\ i_{cr}\end{bmatrix} \quad (1.10)$$

For the rotor:

$$\begin{bmatrix}\Psi_{ar}\\ \Psi_{br}\\ \Psi_{cr}\end{bmatrix} = [L_r] \begin{bmatrix}i_{ar}\\ i_{br}\\ i_{cr}\end{bmatrix} + [Msr] \begin{bmatrix}i_{as}\\ i_{bs}\\ i_{cs}\end{bmatrix} \quad (1.11)$$

$[M_{sr}] = [M_{rs}]^{T}$

$[L_s]$: cyclic inductance matrix in stator.

$[L_r]$:cyclic inductance matrix in rotor.

$[M_{sr}]$:Matrix of stator mutual inductances.

$[M_{rs}]$:Matrix of rotor mutual inductances.

The stator and rotor inductance matrices is:

$$[L_s]=\begin{bmatrix} I_s & M_s & M_s \\ M_s & I_s & M_s \\ M_s & M_s & I_s \end{bmatrix} \quad (1.12)$$

$$[L_r]=\begin{bmatrix} I_r & M_r & M_r \\ M_r & I_r & M_r \\ M_r & M_r & I_r \end{bmatrix} \quad (1.13)$$

The angular position θ between the axes of the stator and the rotor in the matrix of mutual inductances between their phases:

$$[M_{sr}] = [M_{rs}]^T M_0 \begin{bmatrix} \cos(\theta) & \cos(\theta-\frac{2\pi}{3}) & \cos(\theta+\frac{2\pi}{3}) \\ \cos(\theta+\frac{2\pi}{3}) & \cos(\theta) & \cos(\theta-\frac{2\pi}{3}) \\ \cos(\theta-\frac{2\pi}{3}) & \cos(\theta+\frac{2\pi}{3}) & \cos(\theta) \end{bmatrix} \quad (1.14)$$

M_{sr}: stator mutual inductances.

M_{rs}: rotor mutual inductances.

$\boldsymbol{\theta}$: Electric angle relative position between the stator and the rotor axes.

M_0: Maximum mutual inductance.

Using the notion of mutual inductances and the complex notation for sinusoidal quantities at pulsation ωs we can write:

$\Psi_s = L_s I_s + M_{sr} I_r$ (1.15)

$\Psi_r = L_r I_r + M_{rs} I_s$ (1.16)

$V_s = R_s I_s + j\omega_s \Psi_s$ (1.17)

$0 = Rr\ I_r + j\ \omega s\ g\ \Psi_r$ (1.18)

Ls and Lr*:* represent the stator and rotor cyclic inductance respectively,

$M_{rs} = (3/2)\ M_{sr}$ is the cyclic mutual inductance.

c.Mechanical Equation:

The electromagnetic torque can be written by the following equation:

$$T_e=P[I_{s(abc)}]^T \frac{d}{dt}[M_{sr}][I_{r(abc)}] \quad (1.19)$$

To see the full model of the machine, the movement equation of the machine is written as follows:

$$J \frac{d}{dt}\Omega_r=T_e-T_r-f.\Omega \quad (1.20)$$

J: Moment of inertia of rotating masses

T_r: Resistant torque on the machine shaft.

Ω_r: Rotor speed.

T_e: Electromagnetic torque

f: Viscous friction coefficient**.**

The variable coefficients in the equations thus obtained increase the difficulty of solving the model provided by (10) and (12).

This will lead to the application of the park transformation, which will allow these characteristics to be kept constant. [1].

1.10 Clarke transformation:

The Clarke or αβ transform is a space vector transformation of time-domain signals (e.g. voltage, current, flux, etc) from a natural three-phase coordinate system (ABC) into a stationary two-phase reference frame (αβ). It is named after electrical engineer Edith Clarke [5].

$$\begin{bmatrix}X_a\\X_b\\X_c\end{bmatrix}\xrightarrow{c_{23}}\begin{bmatrix}X_\alpha\\X_\beta\end{bmatrix} c_{.a.d}[X_{\alpha\beta}]=c_{23}[X_{abc}] \qquad C_{23}=\frac{2}{3}\begin{bmatrix}1 & -\frac{1}{2} & -\frac{1}{2}\\ 0 & \sqrt{\frac{3}{2}} & -\sqrt{\frac{3}{2}}\end{bmatrix} \quad (I.21)$$

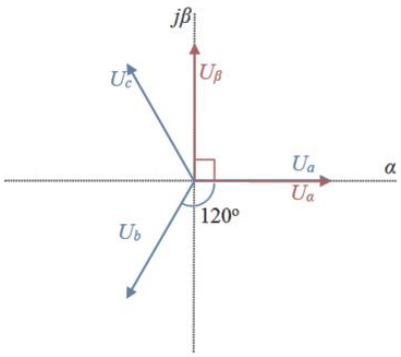

Fig (1.6): Three-phase and two-phase stationary reference frames

U_a, U_b, U_c: the voltage distribution of the three stationary axes.

U_{α}: is the horizontal axis aligned with phase.

U_{β}: the vertical axis rotates by 90 degrees.

The reverse:

$$[x_{abc}] = C_{32}[X_{\alpha\beta}] \text{ with } C_{32} = \begin{bmatrix} 0 & 1 \\ -\frac{1}{2} & \sqrt{\frac{3}{2}} \\ -\frac{1}{2} & \sqrt{\frac{3}{2}} \end{bmatrix} \quad (1.22)$$

1.11 Concordia Transformation

switch from a three-phase abc system to a two-phase αβ system:

$$\begin{bmatrix} x_1 \\ x_2 \\ x_3 \end{bmatrix} \xrightarrow{T_{23}} \begin{bmatrix} x_\alpha \\ x_\beta \end{bmatrix} \quad \text{c to d } [x_{\alpha\beta}] = T_{23}[x_{abc}]$$

$$\text{with} \quad T_{23} = \sqrt{\frac{2}{3}} \begin{bmatrix} 1 & -\frac{1}{2} & -\frac{1}{2} \\ 0 & \sqrt{\frac{3}{2}} & -\sqrt{\frac{3}{2}} \end{bmatrix} \quad (1.23)$$

The reverse:

$$\begin{bmatrix} x_\alpha \\ x_\beta \end{bmatrix} \xrightarrow{T_{32}} \begin{bmatrix} x_1 \\ x_2 \\ x_3 \end{bmatrix} \quad \text{c to d } [x_{abc}] = T_{32}[x_{\alpha\beta}] \quad \text{with} \quad T_{32} = \sqrt{\frac{2}{3}} \begin{bmatrix} 1 & 0 \\ -\frac{1}{2} & \sqrt{\frac{3}{2}} \\ -\frac{1}{2} & -\sqrt{\frac{3}{2}} \end{bmatrix} \quad (1.24)$$

1.12 Park Transformation:

The transformation of the three-phase machine to a two-phase machine consists of replacing any three phase winding (a, b, c) by two equivalent windings, one on the direct axis (d) and the other on the quadrature axis (q), The transformation which translates this passage from the three phase system (a, b, c) to the two-phase system (d, q) is called Park's.

The reference (d, q) is rotating or fixed.

The PARK transformation matrix that preserves instantaneous power is defined [6]:

As follows:

$$\begin{bmatrix} x_0 \\ x_d \\ x_q \end{bmatrix} = \sqrt{\frac{2}{3}} \begin{bmatrix} \cos\Theta & \cos(\theta - 2\pi/3) & \cos(\theta + 2\pi/3) \\ -\sin\Theta & -\sin(\theta - 2\pi/3) & -\sin(\theta + 2\pi/3) \\ \sqrt{\frac{1}{2}} & \sqrt{\frac{1}{2}} & \sqrt{\frac{1}{2}} \end{bmatrix} \begin{bmatrix} x_a \\ x_b \\ x_c \end{bmatrix} \quad \text{(I.25)}$$

In a more compact form:

$$[x_{dq}] = p(\Theta)\,[x_{abc}]$$

$$P(\Theta) = \sqrt{\frac{2}{3}} \begin{bmatrix} \cos\Theta & \cos(\theta - 2\pi/3) & \cos(\theta + 2\pi/3) \\ -\sin\Theta & -\sin(\theta - 2\pi/3) & -\sin(\theta + 2\pi/3) \\ \sqrt{\frac{1}{2}} & \sqrt{\frac{1}{2}} & \sqrt{\frac{1}{2}} \end{bmatrix} \quad \text{(I.26)}$$

the reverse :

$[X_{0dq}] = [P(\theta)]^{-1}\,[X_{abc}]$

$[p(\Theta)]$:The Park direct transformation matrix;

$[p(\Theta)]^{-1}$: The Park inverse transformation matrix;

X : can be voltage, current or flux.

Θ :Rotation angle of the reference (d, q).

The Park reverse transformation matrix is:

$$P(\Theta) = \sqrt{\frac{2}{3}} \begin{bmatrix} \cos\theta & -\sin\theta & \sqrt{\frac{1}{2}} \\ \cos(\theta - 2\pi/3) & -\sin(\theta - 2\pi/3) & \sqrt{\frac{1}{2}} \\ \cos(\theta - 2\pi/3) & -\sin(\theta + 2\pi/3) & \sqrt{\frac{1}{2}} \end{bmatrix} \quad \text{(1.27)}$$

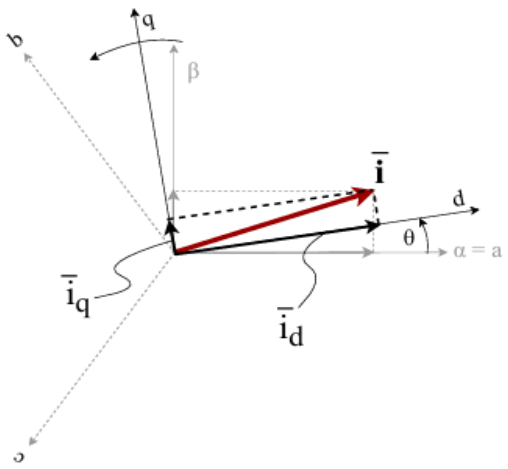

Figure(1.17): Park transformation

1.12.1 Application of the Park transformation:

The transformation of the three-phase machine to a two-phase machine consists in replacing any three-phase winding (a, b, c) by two equivalent windings, one on the direct axis (d) and the other on the quadrature axis (q).

The Park transformation consists in being applied to currents, voltages and fluxes [10].

A. Electrical Equations

$$\begin{cases} V_{sd} = R_s.i_{sd} + \frac{d}{dt}\Psi_{sd} - \omega a\,\Psi_{sq} \\ V_{sq} = R_s.i_{sq} + \frac{d}{dt}\Psi_{sq} - \omega a\,\Psi_{sd} \\ V_{rd} = 0 = R_r.i_{rd} + \frac{d}{dt}\Psi_{rd} - (\omega_a - \omega_r)\Psi_{rq} \\ V_{rq} = 0 = R_r.i_{rq} + \frac{d}{dt}\Psi_{rq} - (\omega_a - \omega_r)\Psi_{rd} \end{cases} \quad (1.28)$$

B. The magnetic Equations

$$\begin{cases} \Psi_{sd} = Ls\,i_{sd} + M_{ird} \\ \Psi_{sq} = Ls\,i_{sq} + M_{irq} \\ \Psi_{rd} = Ls\,i_{rd} + M_{isd} \\ \Psi_{rq} = Ls\,i_{rq} + M_{irq} \end{cases} \quad (1.29)$$

In matrix form:

$$\begin{bmatrix} \Psi_{sd} \\ \Psi_{sq} \\ \Psi_{rd} \\ \Psi_{sq} \end{bmatrix} = \begin{bmatrix} Ls & 0 & M & 0 \\ 0 & Ls & 0 & M \\ M & 0 & Lr & 0 \\ 0 & M & 0 & Lr \end{bmatrix} \begin{bmatrix} i_{sd} \\ i_{sq} \\ i_{rd} \\ i_{rd} \end{bmatrix} \quad (1.30)$$

with:

$L_s = l_s - m_s$: the stator's own cyclic inductance.

$L_r = l_r - m_r$: the rotor's own cyclic inductance.

C. The Mechanical Equation

Applying the Park transformation to the equation gives:

$$T_{em} = P(\Psi_{sd}.i_{qs} - \Psi_{sq}.i_{ds}) \quad (1.31)$$

$$J\frac{d\Omega}{dt} = T_{em} - T_r - f.\Omega \quad (1.32)$$

I.13 The Diagram of the Asynchronous Machine Model:

The asynchronous machine can have different state models. The difference between these models lies in the choice of the state vector X and in the orientation of the reference frame (d, q). The state equation form of the IM is written as[7]:

$$X^{\bullet} = AX + BU \quad (1.33)$$

$$Y = CX + DU \quad (1.34)$$

$$I_{rd} = \frac{\Psi rd - M.Isd}{Lr} \quad (1.35)$$

$$I_{rq} = \frac{\Psi rq - M.Isq}{Lr} \quad (1.36)$$

Let us replace the expressions for the currents Idr and Iqr in equations (35) and (36) by them values in equations (28) Ψ_{sd} and Ψ_{sq} we then obtain:

$$\Psi_{sd} = (Ls - \frac{M_2}{L_r})I_{sd} + \frac{M}{L_r}\Psi_{rd} \quad (1.37)$$

$$\Psi_{sq} = (Ls - \frac{M_2}{L_r})I_{sq} + \frac{M}{L_r}\Psi_{rq} \quad (1.38)$$

By deriving these as, a function of time, we find:

$$\frac{d\Psi_{sd}}{dt} = (L_s - \frac{M2}{L_r})\frac{dI_{sd}}{dt} + \frac{M}{L_r}.\frac{d\Psi_{rd}}{dt} \quad (1.39)$$

$$\frac{d\Psi_{sq}}{dt} = (L_s - \frac{M2}{L_r})\frac{dI_{sq}}{dt} + \frac{M}{L_r}.\frac{d\Psi_{sq}}{dt} \quad (1.40)$$

For the rotor from equations (28) V_{rq} and V_{rd} we obtain:

$$\frac{d\Psi_{rd}}{dt} = -R_r I_{rd} + \omega_r \Psi_{rq} \qquad (1.41)$$

$$\frac{d\Psi_{rq}}{dt} = -R_r I_{rq} + \omega_r \Psi_{rd} \qquad (1.42)$$

By replacing Idr and Iqr with their expressions obtained in (35) and (36) the following expressions are obtained:

$$\frac{d\Psi_{rd}}{dt} = \frac{MR_r}{L_r} I_{sd} - \frac{R_r}{L_r} \Psi_{rd} + \omega_r \Psi_{rq} \qquad (1.43)$$

$$\frac{d\Psi_{rq}}{dt} = \frac{MR_r}{L_r} I_{sq} - \frac{R_r}{L_r} \Psi_{rq} + \omega_r \Psi_{rd} \qquad (1.44)$$

We finally obtain from equations (32) (33), (36) and (37):

$$\frac{dI_{sd}}{dt} = \frac{1}{\sigma L_s} V_{sd} - \left(\frac{R_s}{\sigma L_s} + \frac{M_2 R_r}{\sigma L_s L_{r2}}\right) I_{sd} + \omega I_{sq} + \frac{MR_r}{\sigma L_s L_{r2}} \Psi_{rd} + \frac{M}{\sigma L_s L_{r2}} \omega \Psi_{rq} \quad (1.45)$$

$$\frac{dI_{sq}}{dt} = \frac{1}{\sigma L_s} V_{sq} - \left(\frac{R_s}{\sigma L_s} + \frac{M_2 R_r}{\sigma L_s L_{r2}}\right) I_{sq} + \omega I_{sd} + \frac{MR_r}{\sigma L_s L_{r2}} \Psi_{rq} + \frac{M}{\sigma L_s L_{r2}} \omega \Psi_{rq} \quad (1.46)$$

We can write equations (38) and (39) in the form of state equations such as:

$$\begin{bmatrix} I_{sd} \\ I_{sq} \\ \Psi_{rd} \\ \Psi_{rq} \end{bmatrix} = \begin{bmatrix} -\left(\frac{1}{T_s \sigma} + \frac{1}{Tr}\frac{1-\sigma}{\sigma}\right) & \omega s & \frac{1-\sigma}{\sigma}\frac{1}{MT_r} & \frac{1-\sigma}{\sigma}\frac{1}{M}\omega \\ -\omega_s & -\left(\frac{1}{T_s \sigma} + \frac{1}{Tr}\frac{1-\sigma}{\sigma}\right) & \frac{1-\sigma}{\sigma}\frac{1}{M}\omega & \frac{1-\sigma}{\sigma}\frac{1}{MT_r} \\ \frac{M}{T_r} & 0 & \frac{1}{-T_r} & \omega_r \\ 0 & \frac{M}{T_r} & -\omega_r & -\frac{1}{T_r} \end{bmatrix} \bullet \begin{bmatrix} I_{sd} \\ I_{sq} \\ \Psi_{rd} \\ \Psi_{rq} \end{bmatrix} + \begin{bmatrix} \frac{1}{\sigma L_s} & 0 \\ 0 & \frac{1}{\sigma L_s} \\ 0 & 0 \\ 0 & 0 \end{bmatrix} \bullet \begin{bmatrix} V_{sd} \\ V_{sq} \\ 0 \\ 0 \end{bmatrix} \quad (1.47)$$

With

$T_r = \frac{L_r}{R_r}$, $T_r = \frac{L_s}{R_s}$:Rotor and stator time constant.

$\sigma = 1 - \frac{M_2}{L_s L_r}$: Coefficient de dispersion.

1.14 The Inverter Process of Induction Machine:

I.14.1 Two-level voltage inverter:

he structural diagrams of a three-phase two-level inverter and its load are illustrated in Figure. Each transistor-diode group assembled in parallel forms a Bi controllable switch (on opening and on closing) whose state appears complementary to that associated with it, thus forming a switching arm, for example k11 and k12 [6].

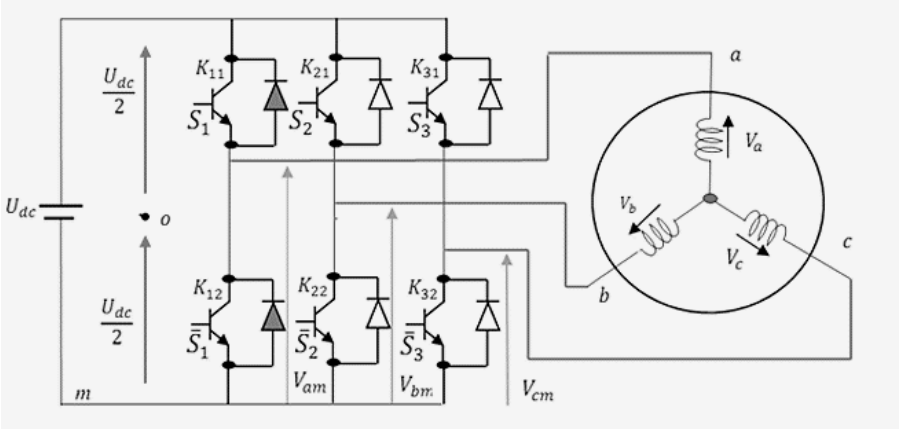

Fig (1.13): Representation of the inverter-IM assembly.

The switch pairs (k11 and k12), (k21 and k22), and (k31 and k32) must be controlled in a complementary manner to ensure the continuity of alternating currents in the load and to prevent short circuiting of the source. The diodes Di (i=1, 2, 6) are freewheeling diodes that protect the transistors.

1.14.2 Modeling of the voltage inverter:

The voltage output of a DC-AC converter can change instantly between 0 and the DC supply voltage, making its instantaneous behavior nonlinear. To apply linear control laws, pulse-width modulation (PWM) is used to generate switching signals that create an output voltage with an average value proportional to a reference signal over a sampling period TT.

This PWM inverter system can be modeled using average values as a linear amplifier, with the duty cycle as input. For more accuracy, it may be represented by a low-pass filter or pure delay to reflect modulation effects [6].

However, this simplified model cannot capture the inverter's fast, nonlinear voltage behavior. For direct nonlinear control, instantaneous modeling is necessary to fully exploit the inverter’s dynamic characteristics.

To simplify the study, let's assume that:

- The switching of the switches is instantaneous.
- The voltage drop across the switches is negligible.
- The load is balanced, connected in a star circuit with an isolated neutral [6].

We therefore have:

Sn = 0; V$ki \neq 0$; top switch open and bottom switch closed.

Sn = 1; Vki = 0; top switch closed and bottom switch open.

he compound voltages Vab, Vbc and Vca are obtained from these relations:

$$\begin{cases} V_{ab} = V_{a0} + V_{b0} = V_{a0} - V_{b0} \\ V_{bc} = V_{b0} + V_{c0} = V_{b0} - V_{c0} \\ V_{ca} = V_{c0} + V_{0a} = V_{c0} - V_{a0} \end{cases} \quad (1.48)$$

Such that V_{a0} , V_{b0} , V_{c0} are the inverter input voltages or DC voltages.

They are referenced relative to a midpoint "o" of a fictitious input divider.

We can write the Charles equations as follows:

$$\begin{cases} V_{a0} = V_{am} + V_{m0} \\ V_{b0} = V_{bm} + V_{m0} \\ V_{c0} = V_{cm} + V_{m0} \end{cases} \quad (1.49)$$

V_{am} , V_{bm} and V_{cm} : are the voltages of the phases of the load (alternating value)

V_{m0} : Neutral voltage of the load relative to the fictitious point "o"

The system V_{an} , V_{bn} and V_{cn} being balanced, it follows:

$$V_{am} + V_{bm} + V_{cm} = 0 \quad (1.50)$$

The substitution of (42) into (43) results in:

$$V_{an} = \frac{1}{3}(V_{a0} + V_{b0} + V_{c0}) \quad (1.51)$$

Replacing (43) in (41), we obtain:

$$\begin{cases} V_{am} = \frac{2}{3} V_{a0} - \frac{1}{3} V_{b0} - \frac{1}{3} V_{c0} \\ V_{bm} = -\frac{1}{3} V_{a0} + \frac{2}{3} V_{b0} - \frac{1}{3} V_{c0} \\ V_{cm} = -\frac{1}{3} V_{a0} - \frac{1}{3} V_{b0} + \frac{2}{3} V_{c0} \end{cases} \quad (1.52)$$

Therefore, the voltage inverter can be modeled by a [T] matrix ensuring the DC-AC transition.

$$[V_{AC}] = [T]\,[V_{dc}] \quad (1.53)$$

Such as :

$$\begin{cases} [V_{ac}] = [V_{am}\ V_{bm}\ V_{cm}]^T \\ [V_{dc}] = [V_{a0}\ V_{b0}\ V_{c0}]^T \\ [V_{dc}] = U_{dc}\,[S_1\ S_2\ S_3]^T \end{cases} \quad (1.54)$$

So, for each arm there are two independent states. These two states can be considered as Boolean quantities.

Assumed ideal switching: Si= (1 ou 0) {i=1,2,3}

The transfer matrix is as follows:

$$[T]=\begin{bmatrix} \frac{2}{3} & -\frac{1}{3} & -\frac{1}{3} \\ -\frac{1}{3} & \frac{2}{3} & -\frac{1}{3} \\ -\frac{1}{3} & -\frac{1}{3} & \frac{2}{3} \end{bmatrix} \quad (1.55)$$

$$\begin{cases} V_{a0} = \frac{U_{dc}}{3}(2S_1 - S_2 - S_3) \\ V_{b0} = \frac{U_{dc}}{3}(2S_2 - S_1 - S_3) \\ V_{c0} = \frac{U_{dc}}{3}(2S_3 - S_1 - S_2) \end{cases} \quad (1.56)$$

By applying the PARK transformation to the phase-neutral voltages given by equation (51), we obtain in the fixed two-phase reference frame the voltage vector as a function of each phase level (52).

$$V_s = V_{s\alpha} + jV_{s\beta} = \sqrt{\frac{2}{3}}\, U_{dc}(S_1 + aS_2 + a^2S_3) \quad (1.57)$$

With

$$\alpha = e^{j\frac{2\pi}{3}} = e^{-j\frac{4\pi}{3}} \quad (1.58)$$

$$a^2 = e^{j\frac{2\pi}{3}} = e^{-j\frac{4\pi}{3}} \quad (1.59)$$

A phase level sequence is defined as each combination of variables S_1, S_2, S_3, giving an element of the set (S_1, S_2, S_3). Since, for the two level inverter, these variables are binary, there are a total of 8 different phase level sequences. illustrates the correspondence between each phase level sequence and the voltage vector, obtained analytically by (57).

We can see the existence of two different phase level sequences (0,0,0) and (1,1,1) giving rise to the same zero voltage vector [6].

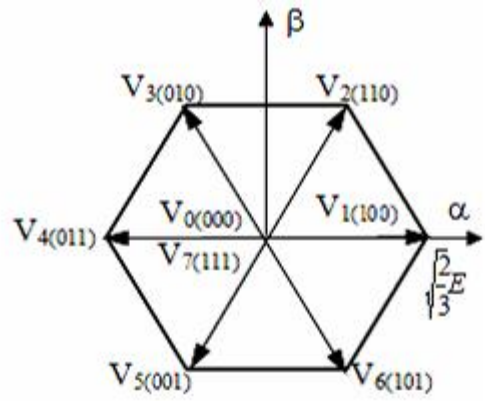

Fig (1.14): Voltage vector and phase level sequences of a 2-level inverter.

1.14.3 Study of the inverter control

Any practical application of an asynchronous drive is linked to precise specifications, requiring a choice of machine power supply mode. There are two power supply modes: current or voltage. This means that the static converter, associated with the machine, imposes a current or voltage of a given shape and amplitude on its stator windings. Depending on the application and the required performance, the power supply type and, consequently, the control system to be implemented will be chosen. Three main designs can be considered [6]:

- Current inverter providing a current supply.
- Voltage inverter providing a voltage supply.
- Voltage inverter providing a current supply.

So, there are several methods for controlling inverter switches. In our work, we will study the voltage control strategy using PWM control [6].

1.15 PWM control strategy

The most commonly used PWM control techniques are: sine-delta PWM control and vector PWM control. The first control uses the principle of intersection between a high-frequency triangular carrier and reference signals called modulator signals to determine the switching instants [6].

At each instant, one of the two switches on each arm is conducting and the other is off. In symmetrical PWM, the reference signal is constant for at least one carrier period. This makes it easy to calculate the times of intersection of the carrier and the modulator at the beginning of

each carrier period. However, symmetrical PWM suffers from underutilization of the DC bus. Indeed, the operating limit is reached for references with an amplitude of V = E/2 [6].

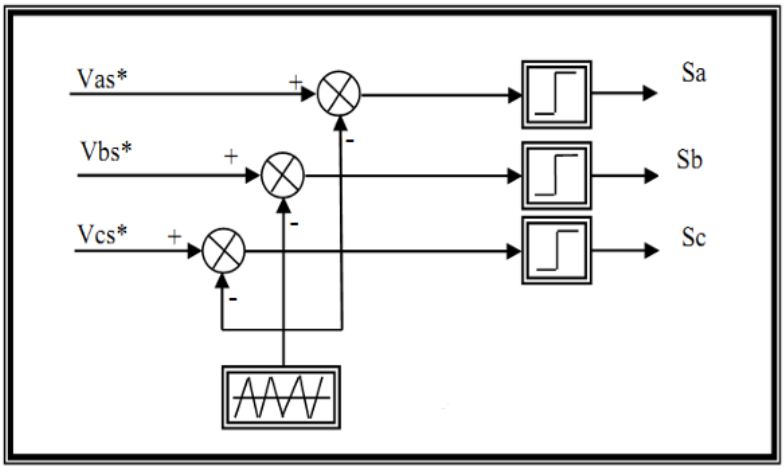

Fig (1.15): Principle of triangular sinusoidal PWM.

1.16 Conclusion

In this chapter, I provided a detailed explanation of the modeling process for both the induction machine and the three phase two level voltage inverter. The mathematical model of the induction machine was developed using PARK's transformation theory, which converts the actual three phase system into an equivalent two-phase system (d.q reference frame).

This transformation significantly simplifies the analysis and mathematical treatment of the machine’s dynamic behavior. the next chapter, where we will explore the principles and different types of control.

Chapter TWO:

Control Techniques for Induction Machine

2.1 INTRODUCTION:

Due to its simple design, low cost, and compatibility with variable speed techniques, the induction machine particularly the squirrel cage type is widely used in variable speed drive applications.

This chapter focuses on speed control methods for squirrel-cage induction motors. One limitation of these machines, compared to DC or synchronous motors, is that a single stator winding supplies both the flux and torque, making control more complex. As a result, motor control must rely on adjusting the waveform parameters either voltage or current.

Speed control systems are generally classified into two categories:

- Constant Frequency Drives, which vary the amplitude of voltage or current
- Variable Frequency Drives, further divided into:

- Scalar Control, which adjusts voltage/current and frequency in a fixed ratio.
- Vector Control, a more advanced technique that enables precise performance by controlling voltage or current components in a rotating frame, or by managing the angle between stator and rotor flux.

The next chapter will detail Direct Torque Control (DTC) two high-performance control strategies for induction motors [6].

2.2 Stator Voltage Variation:

The following figure represents the electromechanical characteristics of an asynchronous machine for three voltage values [6].

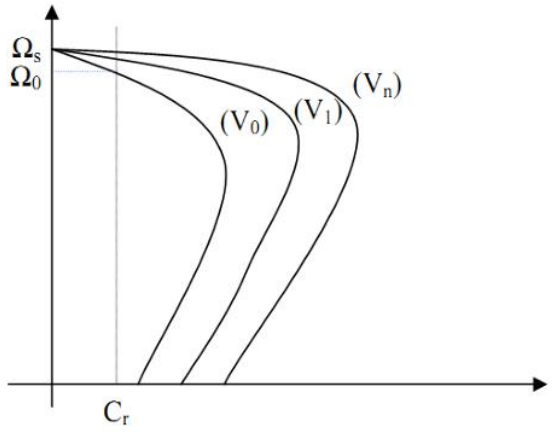

Fig (2.1): torque/speed characteristic for different supply voltages.

Figure (2.1) shows that a decrease in voltage at constant resistive torque causes a decrease in speed, but also a decrease in maximum torque.

This technique has many drawbacks:

- Limitation of the control range
- Decrease in flux and increase in stator current, which causes an increase in Joule losses
- Decrease in torque resistance, which requires oversizing the machine
- The characteristics are not parallel, which is detrimental to machine control
- Low efficiency.

Furthermore, the voltage variation is generally achieved by a dimmer, generating many harmonics on the network and on the machine.

This poses major electromagnetic compatibility problems [6].

2.3 Scalar Control of Induction Machines:

This type of control is one of the oldest methods developed for adjusting the speed of induction motors (IMs)**.** It features a very simple structure and is based on the steady state modeling of the machine. Several scalar control techniques exist, depending on whether the control is applied to the current or the voltage, and they are largely influenced by the type of power converter used (voltage-source or current-source inverter). Today, voltage-source inverters are the most commonly used, especially in low and medium power applications. As a result, the most widely used scalar strategy is the V/f control. Its principle is to maintain a constant voltage to frequency ratio **(**V/f = constant**)**, which ensures that the magnetic flux remains constant

($\Psi_r = V_s/\omega_s$ = constant**).** Torque control is achieved by adjusting the slip, especially under low slip conditions and assuming that the stator resistance voltage drop is negligible [23].

$$T_{max} = \frac{3np}{2N_r}\left(\frac{V_s}{\omega_s}\right)^2 \qquad (2.1)$$

$$\Psi_s = \frac{V_s}{\omega_s} = \text{Cts} \qquad (2.2)$$

$$T_{el} == \frac{3np}{2R_r}\left(\frac{V_s}{\omega_s}\right)^2 \omega_g \qquad (2.3)$$

This equation shows that the torque is directly proportional to the square of the ratio between the stator voltage and frequency**,** which represents the magnetic flux.

At low speeds, the voltage drop across the stator resistance can no longer be neglected. To compensate for this drop, a voltage correction term V_0 is added, known as the compensation term [23].

If $\Omega \leq \Omega_{nom}$, then:

$$\begin{cases} V \;/\; f = \text{Cst} \Rightarrow \Psi = \text{Cst} \\ \text{Temax} = \text{Cst} \end{cases} \qquad (2.4)$$

If the voltage reaches its maximum value and the machine needs to operate at a speed higher than the nominal speed **(**$\Omega > \Omega_{nom}$**),** the voltage is held constant at its nominal value

($Vs = Vs_{nom}$**),** while the frequency is increased. This causes the V/f ratio to decrease, which in turn leads to a reduction in the torque that the machine can produce [23].

This technique is rarely used, mainly due to its limitations particularly the fact that the steady state model used becomes invalid during high-amplitude transient operations, such as starting or reversing the direction of rotation [23].

2.4Advantages and Disadvantages of Scalar Control:

Advantages

- Wide speed variation range.
- Allows the induction motor to maintain a certain level of stability even in the presence of external disturbances or partial system failures.
- Constant flux: $\Psi \approx V_s/f \Rightarrow$ Tem max =constant [23].

Disadvantages

- Performance issues at low speeds due to the voltage drop across the stator resistance Rs×Is
- Slow dynamic response, which results in sluggish torque reaction.
- This method is rarely used due to its limitations**,** mainly because the model used is not valid for high-amplitude transient states, such as during start-up or sudden changes.
- Control is performed only on the magnitude of variables, not on their phase.
- Unsatisfactory speed accuracy, especially under variable load conditions [23].

2.5 Field-Oriented Control (FOC) of Induction Motors:

Field Oriented Control (FOC) technique also known as Vector Control or Decoupled Control used for the precise control of induction motors. Originally introduced by Blaschke in 1972 and further developed by Hasse in 1974, FOC aims to transform the nonlinear model of the induction motor into one that behaves similarly to a separately excited DC motor. In this approach, the magnetic flux is controlled via the excitation current i_{ex}, while the torque is managed through the armature current i_a. This separation enables decoupled control of torque and flux, resulting in high performance during both dynamic and steady-state operations.

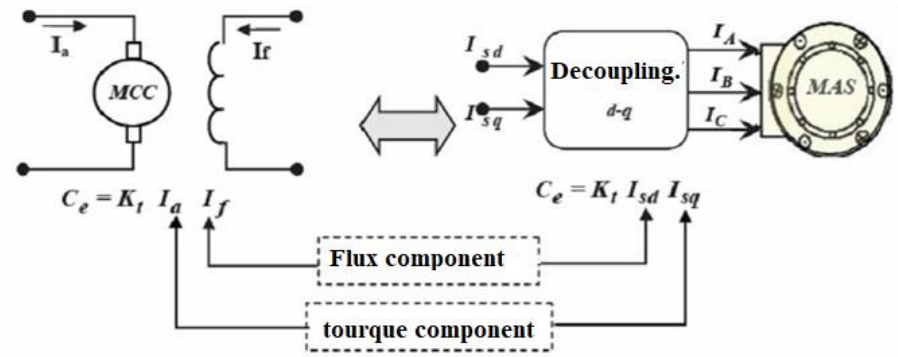

Figure (2.6): Schematic diagram of the decoupling of the IM by analogy with the MCC.

This decoupling allows for faster torque response.

This control is based on the orientation of one of the fluxes: rotor, stator, and air gap. When speaking of flux orientation, it is the d-q axis system that is oriented so that the d axis is in phase with the flux, i.e,This decoupling allows for faster torque response.

$\Psi_{rd}=\Psi_r$

$\Psi_{rq}=0$

Rotor flux orientation vector control is the most widely used because it eliminates the influence of rotor and stator leakage reactances and provides better results than methods based on stator flux orientation or air gap [6].

By imposing, $\Psi_{rq}=0$

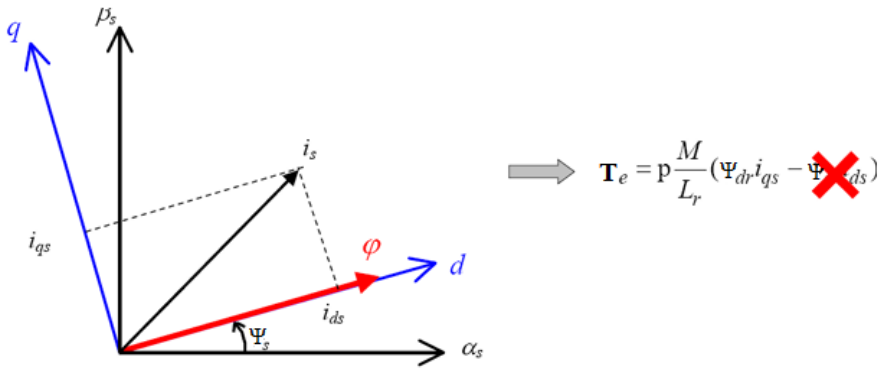

Figure (2.7) Principle of vector control.

Vector control can be implemented using either direct or indirect methods. In the direct method, the Park angle θ_s is computed based on the stator electrical frequency, which is derived from both the rotor speed and the rotor electrical frequency ω_r.

This approach relies on measured or estimated values to determine the Park angle directly.

If flux regulation is not included, the control is considered open loop. In this case, the flux is set through the direct-axis current Ids, and the stator electrical frequency must be estimated using the following equation [6]:

$$\theta_s = \int_0^t (n_p . \Omega + \frac{I_{qs}}{Tr\, I_{ds}})dt \quad \text{or} \quad I_{ds} = \frac{\Psi_r}{M_{sr}} \tag{2.15}$$

2.5.1 Direct Vector Control:

This method, introduced by Blaschke and made public around 1970 (Feedback Control), relies on knowing both the magnitude and position of the rotor flux. To achieve this, several measurements are required at the drive terminals. In Blaschke's approach, the rotor flux is derived from the air gap flux and the stator current. The air-gap flux itself is measured using Hall-effect sensors placed within the stator windings [6].

The calculated rotor flux magnitude is used as feedback in the flux control loop, and the flux orientation makes it possible to project the direct and quadrature current components onto a stationary reference frame.

Although this method does not directly involve the machine's electrical parameters, integrating sensors or additional windings into the stator impacts the cost and durability of the machine, requiring specially designed induction motors and posing challenges due to the temperature sensitivity of the sensors. [6]

As a result, in most cases, rotor flux is estimated using observers or estimators based on available drive measurements. Various implementations can be developed depending on the machine's supply method and the selected reference frame [6].

The control strategy shown in (Figure 2.8) represents a direct vector control scheme, where the rotor flux is regulated according to a defined set point. This approach uses the previously defined estimators for flux and stator angular frequency.

The system includes four PI controllers organized into two decoupled control loops:

- The flux control loop includes a PI flux regulator and an inner current loop that regulates the d-axis stator current (i_{sd}).
- The torque control loop includes a PI speed regulator and an inner current loop that controls the q-axis stator current (i_{sq}) [6]

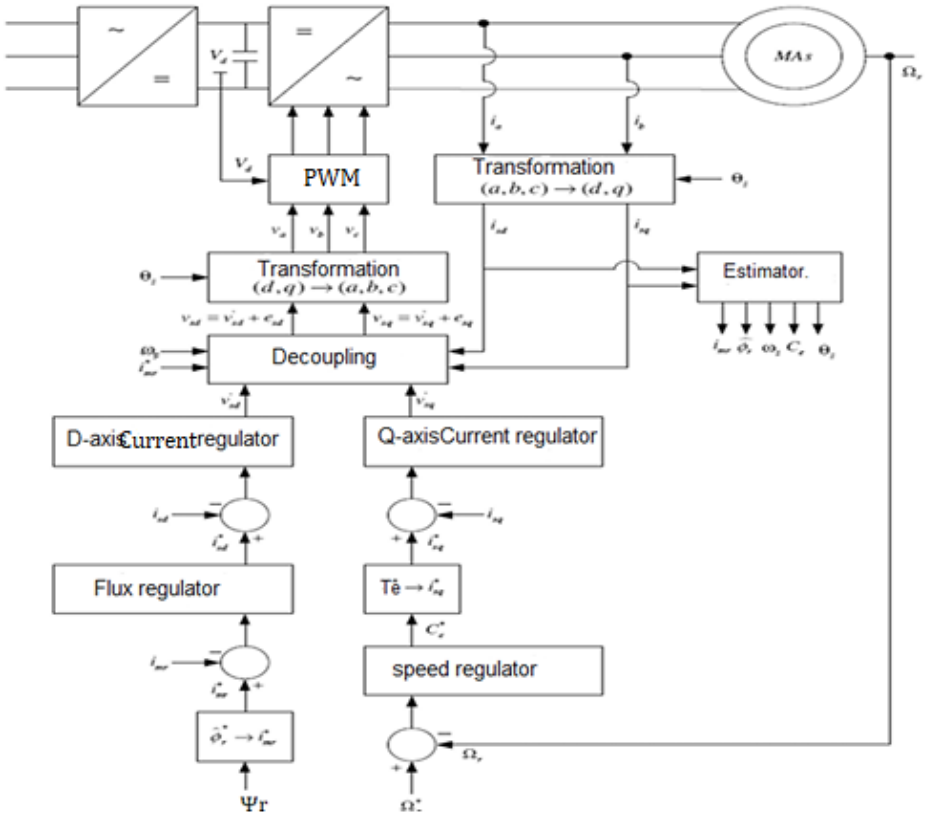

Figure (2.8): Direct vector control of an asynchronous machine.

2.5.2 Indirect Vector Control:

Indirect vector control, introduced by HASSE (feedforward control), is based on the inverse model of the machine, formulated in the rotor flux reference frame. In this method, when the machine is controlled by current, decoupling is naturally achieved, as the torque and flux can be independently managed through the stator current vector components similar to the control structure of a DC motor [6].

A common strategy involves keeping the ids component constant to maintain a fixed, nominal flux in the machine. The ids current regulator ensures that the actual current remains equal to its reference value ids* [6].

With constant flux, torque can be adjusted by modifying the i_{qs} component. To accelerate the machine and increase speed, a positive reference i_{qs}^* is applied. The i_{qs} current regulator enforces this reference, producing a positive torque. This reference i_{qs}^* can also be generated automatically by a speed controller, which compares the actual speed with the desired speed Ω^* and adjusts the torque (and thus i_{qs}^*) accordingly. [6]

(Figure 2.8) illustrates this control structure, showing the vector control diagram for the asynchronous machine. It includes speed regulation and two current control loops for ids and iqs , with outputs providing the voltage references $V_{ds}*$ and V_{qs}^* in the (d q) reference frame [6].

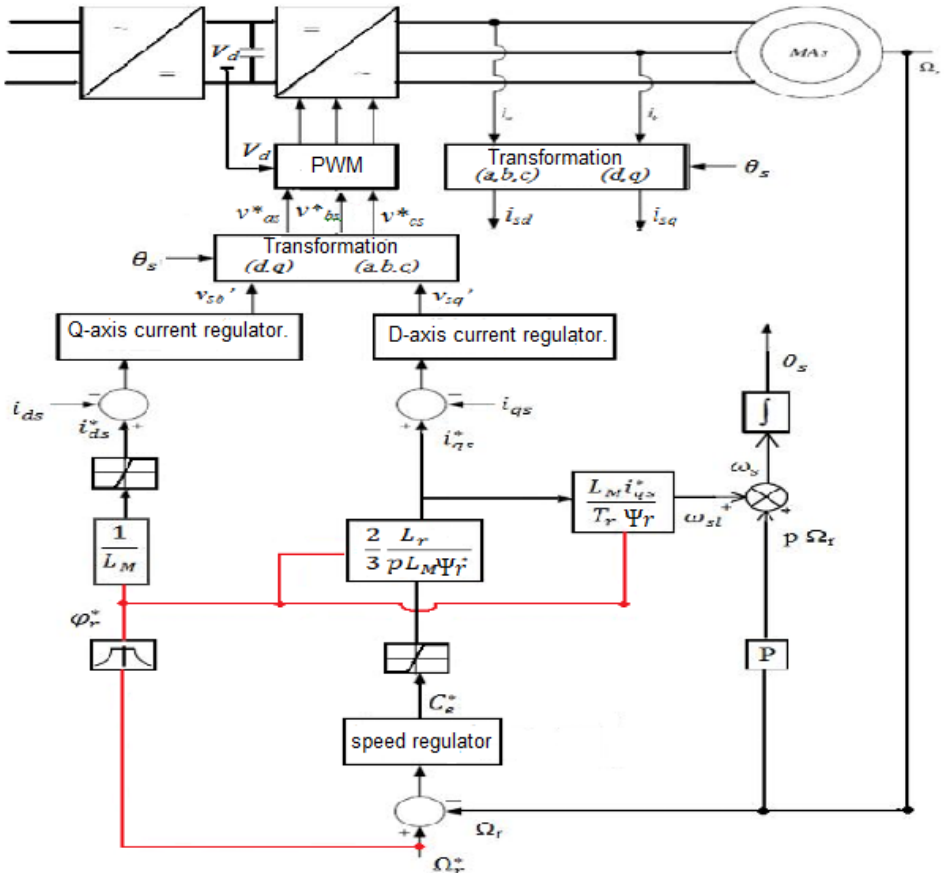

Figure (2.9): Indirect vector control of an asynchronous machine.

2.6 Advantages and Disadvantages of Vector Control (FOC):

Advantages:

- Effective in both steady-state and transient operating conditions.
- Decoupling between torque and flux components, allowing independent control.
- Fast torque response, enabling quick adaptation to load changes.
- Control is performed in terms of both magnitude and phase, improving precision.
- High accuracy in controlling speed and torque.

Disadvantages:

- Low robustness to parameter variations (e.g., due to temperature or magnetic saturation).
- Requires significant computational resources and accurate motor parameter identification.
- High cost, due to the need for sensors (e.g., speed and flux sensors).

2.7 Direct Torque Control :

Direct torque control (DTC) of asynchronous machines is an increasingly used technique for controlling the voltage inverter combination. It is based on a pulse-width modulation (PWM) power supply and on decoupling the motor flux and torque. In a frame of reference linked to the stator, the instantaneous values of the stator flux and electromagnetic torque are estimated from the stator values. Using hysteresis comparators, the flux and torque are controlled directly and independently with an appropriate selection of the voltage vector imposed by the inverter. In the following chapter, we will detail this control technique [6].

2.8 CONCLUSION:

In this chapter, we first reviewed the main controls used for asynchronous machines. We presented scalar, vector, and DTC controls.

Variable frequency allows the asynchronous motor to operate beyond its rated speed, but this reduces the maximum torque. Scalar control overcomes this problem by keeping the maximum torque constant. Although this technique has its drawbacks, it does not allow dynamic torque control, especially at low frequencies. Vector control offers very high dynamic and static performance, but it has the major drawback of being sensitive to parametric variations in the machine, which degrades the robustness of the control model.

Direct torque control, which we will study later, does not require decoupling between flux and torque.

Chapter Three:
Direct Torque Control of an Induction Machine

3.1 Introduction

So, the whole idea of Direct Torque Control, or DTC, goes way back to 1985, thanks to Takahashi. Ever since then, a lot of smart folks have done a ton of work to really understand and model how this thing works.

The cool thing about DTC is that it lets you figure out the control settings specifically, how much magnetic flux the motor has and how much torque it's producing just by looking at the motor's current. You don't even need those separate mechanical sensors to measure speed or position!

The way DTC methods work is by directly telling the inverter's switches what to do. It makes these decisions based on those pre-calculated values of the motor's magnetic flux and torque. So, instead of the inverter just following a set pattern of voltage or frequency like in older PWM control methods, the switching changes are directly tied to what's actually happening inside the motor electrically, Basically, the goal of controlling those switches is to point the motor's magnetic field in the exact direction we want it to go, based on what we've set as the target values. In this chapter, we're going to walk through the basic ideas behind Direct Torque Control for induction motors (IMs) and show you what happens in simulations [22].

3.2 The Principle of DTC Control

Direct Torque Control (DTC) is based on the direct selection of the switching sequence to be applied to a voltage inverter. This selection is generally carried out using hysteresis controllers, which are responsible for monitoring the system's state, particularly the amplitude of the stator flux and the electromagnetic torque.

Based on these values, the optimal stator voltage vector to be applied to the asynchronous machine can be determined in order to keep the torque and flux within their respective hysteresis bands.

Another factor influencing the voltage selection is the position of the stator vector in the complex plane, which is typically divided into six or twelve sectors.

Figure (3.1) provides a schematic illustration of this method, showing the flux and torque estimators, as well as the two- and three-level flux and torque controllers, respectively, as originally proposed by Takahashi. [22]

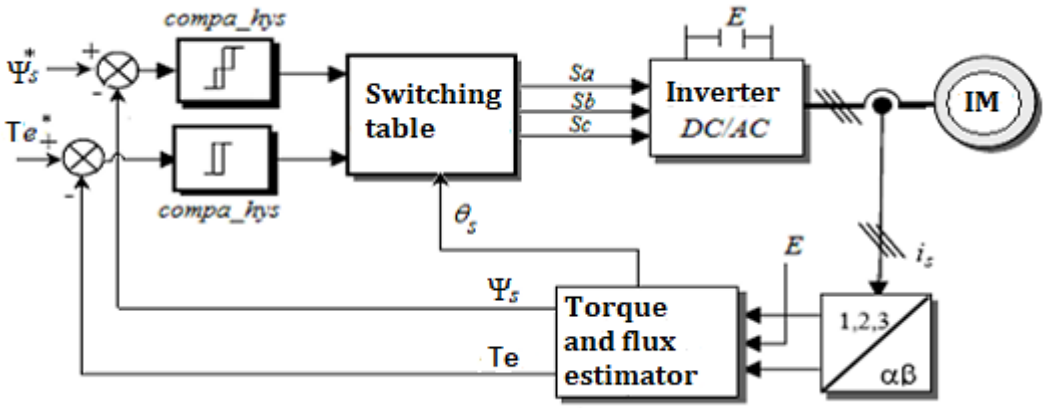

Figure (3.1): The DTC command strategy

3.3 Advantages and Disadvantages of DTC:

a. Advantages:

The advantages of DTC include:

− It does not require calculations in the rotor frame (d, q).

− Excellent torque dynamics,

− Good robustness with respect to variations in machine parameters,

− No use of Park transforms and their inverse,

− No need for PWM voltage modulation calculation blocks,

− No decoupling of currents from control voltages.

− The rotor position angle is not necessary to know; only the sector in which the stator flux is located is necessary[22].

b. Disadvantages:

The disadvantages of DTC control can be summarized in the following points:

− The existence of often significant torque and flux ripples,

− The switching frequency is not controlled,

− The need to use stator flux and torque estimators,

− Stator currents are poorly controlled during transient conditions [22].

3.4 Electromagnetic Torque and Stator Flux Control:

3.4.1 Principle Electromagnetic Torque Control:

The vector expressions for the stator voltage and rotor voltage of the induction machine in a fixed frame of reference linked to the stator are given by:

$$\begin{cases} \overline{Vs} = R_s I_s + \frac{d}{dt}\overline{\Psi_s} \\ \overline{Vr} = 0 = R_r I_r + \frac{d}{dt}\Psi_r - j\omega\,\overline{\Psi_r} \end{cases} \quad (3.1)$$

On the other hand, from the expressions for the fluxes in a fixed frame linked to the stator, we can express the rotor current expression:

$$\begin{cases} \overline{\Psi_s} = L_s\,\overline{i_s} + M\,\overline{i_r} \\ \overline{\Psi_r} = L_r\,\overline{i_r} + M\,\overline{i_s} \end{cases} \quad (3.2)$$

$$\Rightarrow \overline{i_r} = \frac{1}{\sigma Lr}\left(\overline{\Psi_r} - \frac{M}{Ls}\overline{\Psi s}\right) \quad (3.3)$$

With: $\sigma = \left(1 - \frac{M^2}{L_r L_s}\right)$:(dispersion coefficient).

Equation (3.5) becomes:

$$Vs = R_s I_s + \frac{d}{dt}\Psi_s \quad (3.4)$$

$$\frac{d}{dt}\Psi_r + \left(\frac{1}{\sigma\,\tau_r} - j\omega\right)\Psi_r = \frac{M}{L_s}\frac{1}{\sigma\,\tau_r}\,\Psi_s \qquad (3.5)$$

$\tau_r = \frac{L_r}{R_r}$ (Rotor time constant).

These system relationships show that:

−It is possible to control the vector Ψ_s from the vector Vs to the voltage drop $R_s.I_s$ near.

− The rotor flux vector Ψ_r follows the variations of the stator flux Ψ_s with a small delay caused by the time constant $\sigma\,\tau_r$.

− The rotor of the machine behaves as a "filter of time constant $\sigma\,\tau_r$ between the stator flux and the rotor flux of the asynchronous machine.

If we report in the expression of electromagnetic torque, by setting the angle $\delta = (\overline{\Psi_s}\ , \overline{\Psi_r})$, the torque is expressed by:

$$Te = n_p \frac{M}{Tr\ L_s}(\Psi_s\ .\ \Psi_r) = n_p \frac{M}{\tau_r\ Ls}\|\Psi_s\|.\ \|\Psi_r\|\sin\delta \qquad (3.6)$$

$\|\Psi_s\|$:Stator flux vector modulus.

$\|\Psi_r\|$:rotor flux vector modulus.

δ: angle between the stator flux and rotor flux vectors.

The torque error is defined by the difference between the references values of the torque and the actual estimated values:

The torque depends on the magnitude of two vectors, Ψ_s and Ψ_r , and their relative position. If we can precisely control the flux Ψ_s in terms of both magnitude and position using $\overline{V_s}$, then it becomes possible to control both the amplitude and the relative position of $\Psi_s$and Ψ_r, and therefore the torque. Of course, this is only feasible if the control period T_e of the voltage V_s is much shorter than the time constant σ[23].

3.4.2 Principles of Stator Flux Control

Direct torque control is based on the orientation of the stator flux. The expression for the stator flux in the stator reference frame of the machine is given by the following equation:

$$\overline{\Psi_s}(t)=\int_0^t(\overline{V}_s.-R_s\overline{I}_s)dt+\overline{\Psi}_{s0} \quad (3.7)$$

During a control period [0, Te] corresponding to the sampling period T_e expression (3.9) can be written as follows:

$$\overline{\Psi_s}(t)=\overline{\Psi}_{s0}+\overline{V}_s\ T_e-\int_0^t(R_s\overline{I}_s)dt \quad (3.8)$$

$\overline{\Psi}_{s0}$: is the flux vector at t=0

A non zero voltage vector is applied to the machine, and the term $R_s\overline{I_s}$ is considered negligible compared to the voltage $\overline{V_s}$. This assumption holds true when the rotational speed is sufficiently high.

We will have:

$$\overline{\Psi_s}(t)=\overline{\Psi}_{s0}+\overline{V_s}\ T_e \quad (3.9)$$

$$\overline{\Psi_s}(t)-\overline{\Psi}_{s0}=\Delta\overline{\Psi_s}=\overline{V_s}\ T_e \quad (3.10)$$

Equation (3.10) is illustrated in Figure (3.1), which shows that the tip of the flux vector $\Psi_s(t)$ moves along a straight line in the direction defined by the applied stator voltage vector[23].

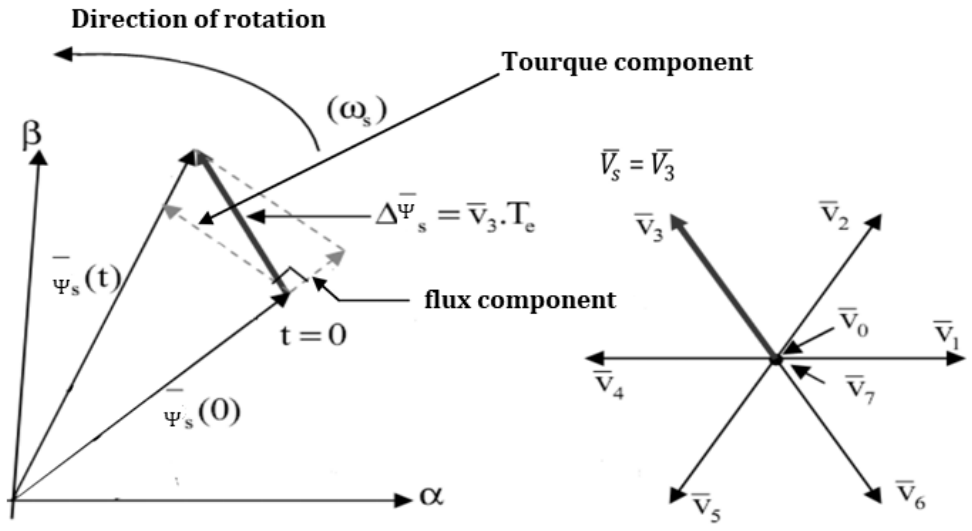

Figure (3.2): Evolution of the tip of $\Psi_s(t)$ assuming $R_s I_s$ is negligible.

The radial component of the voltage vector influences the amplitude of the stator flux vector $\overline{\Psi_s}$, while its tangential component affects the position (or angle) of $\overline{\Psi_s}$. By selecting an appropriate sequence of voltage vectors $\overline{V_s}$ over the control period T_e, and keeping $\overline{V_s}$ approximately constant, the tip of the stator flux vector $\Psi\bar{s}$ can follow a nearly circular trajectory provided that T_e is much shorter than the period of stator flux rotation.

When the applied voltage vector $\overline{V_s}$ is defined by the derivative $\frac{d\overline{\Psi_s}}{dt}$ and is non-zero, the direction of motion of the tip of the stator flux vector $\overline{\Psi_s}$ is determined by the chosen $\overline{V_s}$.

Neglecting the term $R_s\bar{I}_s$, the voltage vector can be approximated as $\overline{V_s} \approx \frac{d\overline{\Psi_s}}{dt}$. Therefore, both the rotational direction and speed of the stator flux vector depend heavily on the selection of $\overline{V_s}$[23].

3.5 Estimation of stator flux and electromagnetic torque

3.5.1 Stator flux estimation

The estimation of the stator flux is usually performed by integrating the back electromotive force (back EMF). The stator flux components can be represented using stator voltages and currents in the stationary reference frame (α, β) as follows [23]:

$$\begin{cases} \Psi_{s\alpha} = \int_0^t (V_{s\alpha} - R_s\, I_{s\alpha})dt \\ \Psi_{s\beta} = \int_0^t (V_{s\beta} - R_s\, I_{s\beta})\, dt \end{cases} \quad (3.11)$$

The stator flux magnitude and flux angle can be computed as:

$$|\Psi_s| = \sqrt{\Psi_{s\alpha} + \Psi_{s\beta}} \quad (3.12)$$

$$\Theta_s = \tan^{-1}(\Psi_{s\beta}/\Psi_{s\alpha}) \quad (3.13)$$

The stator voltage components ($V_{s\alpha}$ $V_{s\beta}$) are obtained by applying Concordia transformation on the output voltage of the three-phase V_{SI}.

$$\begin{bmatrix} V_{s\alpha} \\ V_{s\beta} \end{bmatrix} = \begin{bmatrix} 1 & -\frac{1}{2} & -\frac{1}{2} \\ 0 & \sqrt{\frac{3}{2}} & -\sqrt{\frac{3}{2}} \end{bmatrix} \quad (3.14)$$

The output voltages of VSI which are the input stator voltages of the IM are given by:

$$\begin{cases} V_{sa} = \frac{V_{dc}}{3}(2S_a - S_b - S_c) \\ V_{sb} = \frac{V_{dc}}{3}(2S_b - S_c - S_a) \\ V_{sc} = \frac{V_{dc}}{3}(2S_c - S_a - S_b) \end{cases} \quad (3.15)$$

The stator current components ($i_{s\alpha}$, $i_{s\beta}$) can also be derived by applying the Concordia transformation to the measured phase currents:

$$\begin{cases} i_{s\alpha} = \sqrt{\frac{2}{3}}\, i_{sa} \\ i_{s\beta} = \frac{1}{\sqrt{2}}\,(i_{sb} - i_{sc}) \end{cases} \quad (3.16)$$

3.5.2 Electromagnetic torque estimation

The electromagnetic torque generated by the induction motor can be calculated using the cross product of stator quantities, specifically the stator flux and stator current vectors. The torque is given by the following expression:

$$T_{em}=n_p(\Psi_{s\alpha}\, I_{s\beta}-\Psi_{s\beta}\, I_{s\alpha}) \quad (3.17)$$

3.6 Development of the Control Vector for DTC:

3.6.1 Development of the Flux Controller:

this type of controller, it becomes easy to regulate and keep the tip of the flux vector within a circular ring, as illustrated in Figure (3.4). Moreover, the controller has a single input and a single output, which determines the direction of change of the stator flux magnitude $\bar{\Psi}_s$, in order to select the appropriate voltage vector. The output of the controller is a Boolean variable (Cflx), which directly indicates whether the flux amplitude should be increased (Cflx = 1) or decreased (Cflx = 0) to maintain the desired value [48,49]. Equation (3.20) represents the mathematical form of the two level hysteresis comparator used for stator flux control [23].

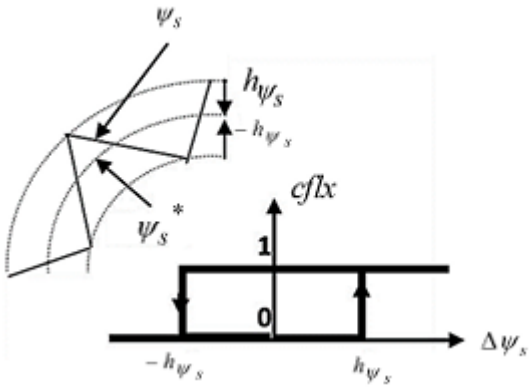

Fig.(3.3) Tow-level hysteresis comparator for stator flux control.

$$\begin{cases} \text{si} \quad \varepsilon_\Psi > \Psi_s & so\ cflx = 1 \\ \text{si } 0 \leqslant \varepsilon_\Psi \leqslant \Delta\Psi_s \text{ and } \frac{d\Psi_s}{dt} > 0 & so\ cflx = 0 \\ \text{si } 0 \leqslant \varepsilon_\Psi \leqslant \Delta\Psi_s \text{ and } \frac{d\Psi_s}{dt} < 0 & so\ cflx = 1 \\ \text{si} \quad \varepsilon_\Psi < -\Psi_s & so\ cflx = 0 \end{cases} \tag{3.18}$$

With:

$$\varepsilon_{\Psi s} = \Psi_{s\,ref} - \Psi_s$$

$\Psi_{s\,ref}$: The reference value of the stator flux.

$\Delta\Psi_s$: The hysteresis band width of the flux controller.

$cflx$: Represents the output state of the hysteresis comparator.

3.6.2 Development of the Torque Controller:

The purpose of the torque controller is to keep the electromagnetic torque within permissible limits, defined as:

$$|T_{emref} - T_{em}| \leqslant \Delta T_{em} \tag{3.19}$$

Where:

T_{emref}**:** The desired or target value of the electromagnetic torque.

ΔT_{em}**:** The width of the hysteresis band used by the torque controller.

the torque can be either positive or negative depending on the machine's direction of rotation. Therefore, it is necessary to use either a two level or three level hysteresis controller for proper torque regulation [23].

A. Two-Level Torque Controller:

This controller operates in a similar manner to the one used for regulating the flux vector. A two-level controller is employed when torque control is required in only one direction of rotation. In this case, only the voltage vectors V_{i+1} ,V_{i+2}, and the zero voltage vectors are used to influence the behavior of the flux vector. Torque reduction is achieved by selecting the zero voltage vectors[23].

B. Three-Level Torque Controller

The three-level hysteresis comparator (-1, 0, 1) allows the motor to be controlled in both directions of rotation, either for a positive or negative torque. This controller is modeled by the algorithm, where Tcpl represents the output state of the comparator and ΔT_{em} is the hysteresis band width (see Figure 3.4)[23]:

The Mathematical Form of the Three Level Hysteresis Comparator for Electromagnetic Torque [23]:

$$\begin{cases} \varepsilon_t > \Delta T_{em} & \Rightarrow \quad Tcpl = 1 \\ 0 \leq \varepsilon_t \leq \Delta T_{em} \text{ and } \frac{d\varepsilon_t}{dt} > 0 & \Rightarrow \quad Tcpl = 0 \\ 0 \leq \varepsilon_t \leq \Delta T_{em} \text{ and } \frac{d\varepsilon_t}{dt} < 0 & \Rightarrow \quad Tcpl = 1 \\ \varepsilon_t < -\Delta T_{em} & \Rightarrow \quad Tcpl = -1 \\ -\Delta T_{em} \leq \varepsilon_t \leq 0 \text{ and } \frac{d\varepsilon_t}{dt} > 0 & \Rightarrow \quad Tcpl = 0 \\ -\Delta T_{em} \leq \varepsilon_t \leq 0 \text{ and } \frac{d\varepsilon_t}{dt} < 0 & \Rightarrow \quad Tcpl = -1 \end{cases} \tag{3.20}$$

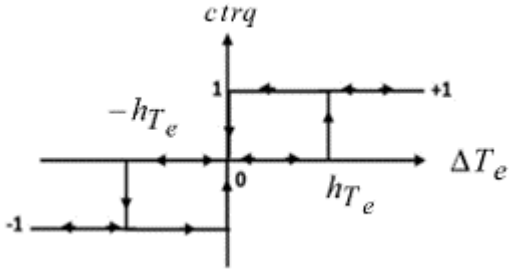

Fig:(3.4) Three level hysteresis comparator for electromagnetic torque control

3.7 Switching Table Construction and Control Algorithm Design :

3.7.1 Six sector Switching table:

To achieve decoupled control, a pair of hysteresis comparators is used to process the stator flux and torque errors. The outputs of these comparators guide the selection of the appropriate

voltage vector. However, this selection depends not only on the comparator outputs but also on the position of the stator flux vector. As a result, the circular trajectory of the stator flux vector is divided into six symmetrical sectors.

where:

sector1: $\frac{11\pi}{6} < \theta s < \frac{\pi}{6}$, sector2: $\frac{\pi}{6} < \theta s < \frac{\pi}{2}$,……..sector6: $\frac{3\pi}{2} < \theta s < \frac{11\pi}{6}$.

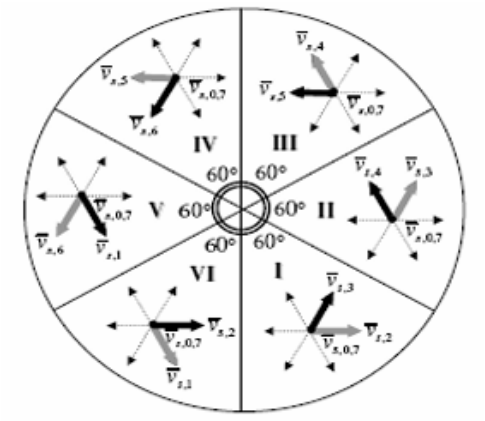

Fig.(3.5) Voltage vector selection when the stator flux vector is located in sector i.[26]

While the stator flux vector is located in the sector i we have:

If i V_{i+1} is selected, Ψ_s increases and T_{em} increases.

If i V_{i-1} is selected, Ψ_s increases and T_{em} decreases..

If i V_{i+2} is selected,Ψ_s decreases and T_{em} increases.

If i V_{i-2} is selected, Ψ_s decreases and T_{em} decreases.

In each sector, the voltage vectors V_i and V_{i+3} are excluded from selection because they can either increase or decrease the torque within the same sector, depending on the stator flux vector's position in the first or second half of the sector. When the zero voltage vectors V_0 and V_7 are applied, the stator flux vector will stop moving and its magnitude stays constant. This causes a reduction in electromagnetic torque, though the decrease is less significant compared to when active voltage vectors are used. The resulting DTC look-up table, originally proposed by Takahashi, is shown in Table (3.1)[1].

Error	sector	I	II	III	IV	V	VI
Cflx=1	Ctrq=1	V_2	V_3	V_4	V_5	V_6	V_1
	Ctrq=0	V_7	V_0	V_7	V_0	V_7	V_0
	Ctrq=-1	V_6	V_1	V_2	V_3	V_4	V_5
Cflx=0	Ctrq=1	V_3	V_4	V_5	V_6	V_1	V_2
	Ctrq=0	V_0	V_7	V_0	V_7	V_0	V_7
	Ctrq=-1	V_5	V_6	V_1	V_2	V_3	V_4

Table (3.1) Look-up table for basic direct torque control.

3.7.2 DTC improvement using twelve sectors switching table:

In conventional six-sector DTC, two switching states per sector are typically not utilized, leading to ambiguity in torque control. To address this, sector shifting is applied by redefining the first sector to span from (0 to $\frac{\pi}{3}$) instead of($\frac{11\pi}{6}$ to $\frac{\pi}{6}$) from , resulting in a new switching table. However, even with this modification, two voltage vectors per sector specifically (V_{i+2} V_{i-1}) remain unused, which present an ambiguity in flux instead of torque.

Another strategy divides the circular flux locus into 12 sectors instead of 6 as shown in Fig (3.6) This makes all the six states used per sector [23].

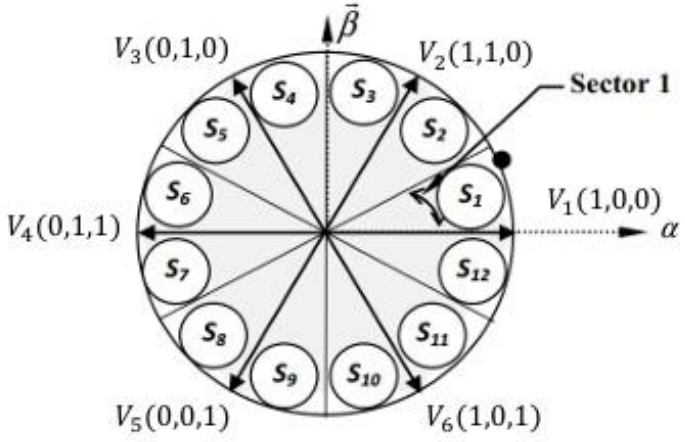

Fig(3.6)Voltage space vector in 12 sectors case

In twelve-sector DTC, voltage vector V1causes a significant increase in flux and only a slight increase in torque within sector 12. Conversely, V2 results in a substantial torque increase with minimal impact on flux. This highlights the need to distinguish between small and large torque

variations. To achieve this, the torque hysteresis band is divided into four levels. Consequently, a twelve sector look-up table is developed, as shown in Table (3.2)[1].

Error	Sector	I	II	III	IV	V	VI	VII	VIII	IX	X	XI	XII
Cflx=1	Ctrq=2	V_2	V_3	V_3	V_4	V_4	V_5	V_5	V_6	V_6	V_1	V_1	V_2
	Ctrq=1	V_2	V_2	V_3	V_3	V_4	V_4	V_5	V_5	V_6	V_6	V_1	V_1
	Ctrq= -1	V_1	V_1	V_2	V_2	V_3	V_3	V_4	V_4	V_5	V_5	V_6	V_6
	Ctrq=-2	V_6	V_1	V_1	V_2	V_2	V_3	V_3	V_4	V_4	V_5	V_5	V_6
Cflx=0	Ctrq=2	V_3	V_4	V_4	V_5	V_5	V_6	V_6	V_1	V_1	V_2	V_2	V_3
	Ctrq=1	V_4	V_4	V_5	V_5	V_6	V_6	V_1	V_1	V_2	V_2	V_3	V_3
	Ctrq= -1	V_5	V_5	V_6	V_6	V_1	V_1	V_2	V_2	V_3	V_3	V_4	V_4
	Ctrq=-2	V_5	V_6	V_6	V_1	V_1	V_2	V_2	V_3	V_3	V_4	V_4	V_5

Table (3.2) Look up switching table with twelve sectors.

Numerous studies in the literature have indicated that increasing the number of sectors has only a modest effect on reducing torque ripple and current harmonics. However, twelve-sector DTC offers improved dynamic performance across both high and low speed operating regions Therefore, the twelve-sector DTC approach is selected over the six-sector version for simulation and real-time implementation in this chapter[1].

3.8. The Direct Torque Control (DTC) strategy:

The core principle of this control strategy lies in directly regulating the electromagnetic torque and stator flux of the machine using hysteresis controllers. The objective is to maintain both the stator flux and the electromagnetic torque within predefined hysteresis bands. A schematic representation of this technique is shown in Figure (3.7), which illustrates the flux and torque estimators, as well as their respective hysteresis controllers.

It is important to note that in Direct Torque Control (DTC), using a high sampling (computation) frequency is recommended to minimize torque ripple, which is a common side effect of hysteresis-based regulation [22].

3.9. Global scheme of basic direct torque control:

The overall control scheme of the basic Direct Torque Control (DTC) strategy is illustrated in Fig. (3.7) It includes the following components: a speed regulation loop utilizing a PI controller,

independent flux and torque hysteresis controllers, a switching look up table, a Voltage Source Inverter (VSI) connected to an induction motor, voltage and current processing blocks with 3/2 (Concordia) transformation, as well as flux and torque estimators with sector and position detection [24].

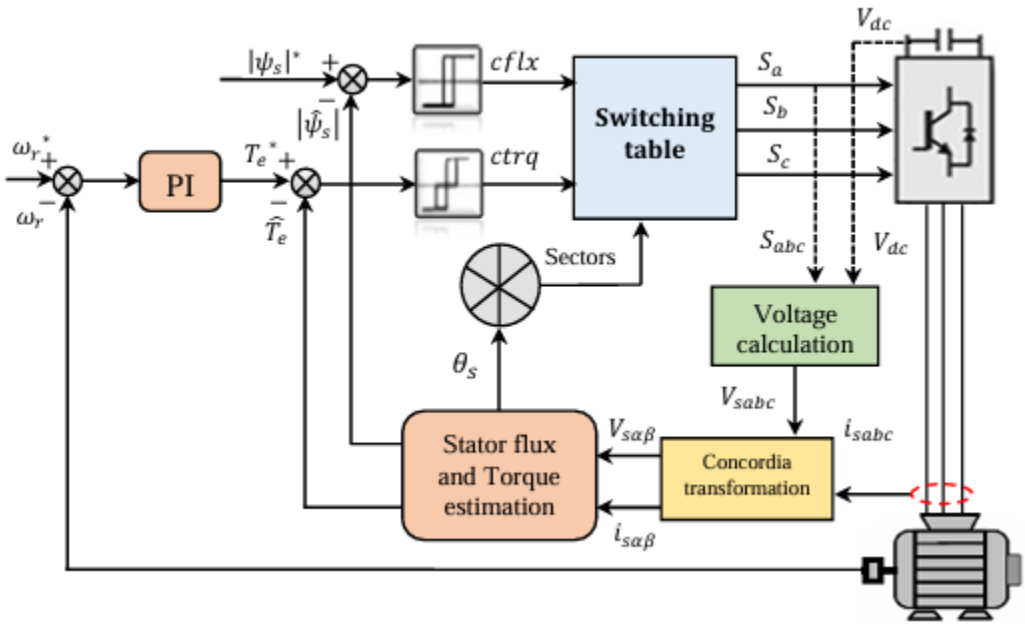

Fig(3.7) Global control scheme of basic direct torque control.

3.10. Simulation Results

The structural behavior of the direct torque controllers proposed in this chapter for controlling a 3 kW asynchronous motor powered by a two level inverter is simulated in the Matlab/Simulink environment. A comparative study between the12 sector DTC and the conventional 6 sector DTC is presented, the PI speed controllers are configured with the same parameters. The sampling time is set to 10−5 s with fixed step. To ensure a evaluation between the two methods.The machine and controller parameters are listed in Appendix A. Different operating conditions are used for the two control methods.

We will study this technique in two cases: the first with six sectors and the second with 12 sector. We will compare them in terms of speed, current, flux, and torque when there is a load, when there is no load, and when the motor is rotating in the opposite direction. We will see the difference between the two cases in all the situations we discussed.

3.10.1 with no load application:

This section presents the starting up state of the induction motor according to speed step reference of 1000 rpm. With no load of 0 N.m. Figs.(3. 8,9,10,11,12) show respectively rotor speed, torque, stator phase current isa with THD analysis, stator flux. The figures are specified: (a) for DTC 6 sectors, and (b) for DTC 12 sectors.

a) b)

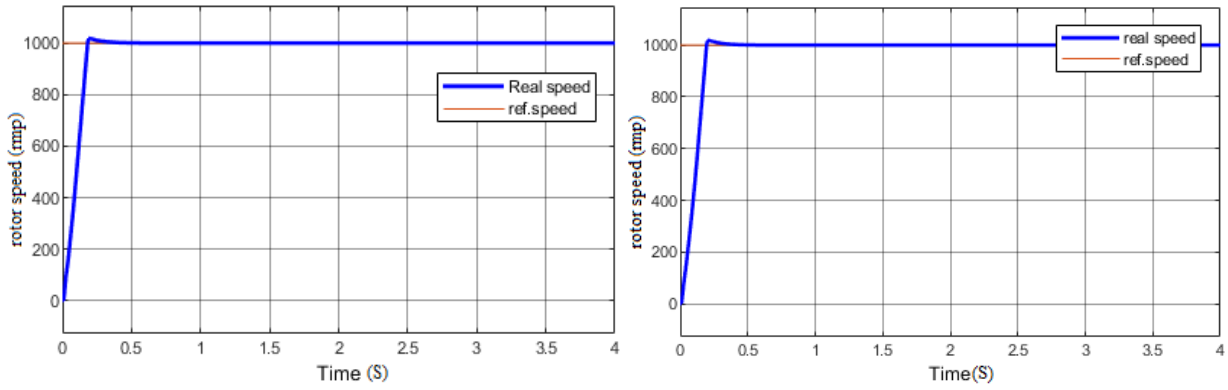

Fig(3.8) Rotor speed response at the starting up and steady states with no load application.

a) b)

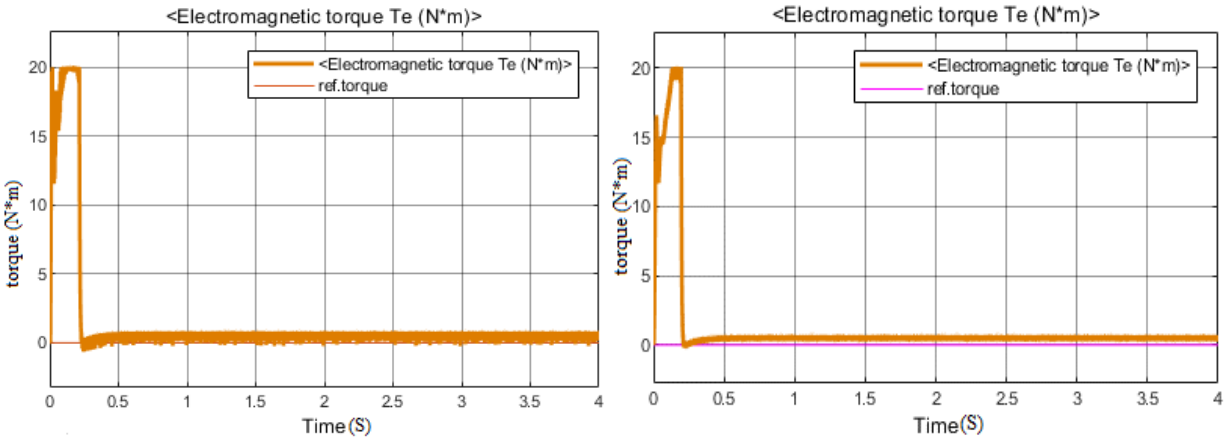

Fig.(3.9) Electromagnetic torque with no load application of 0 N.m .

a) b)

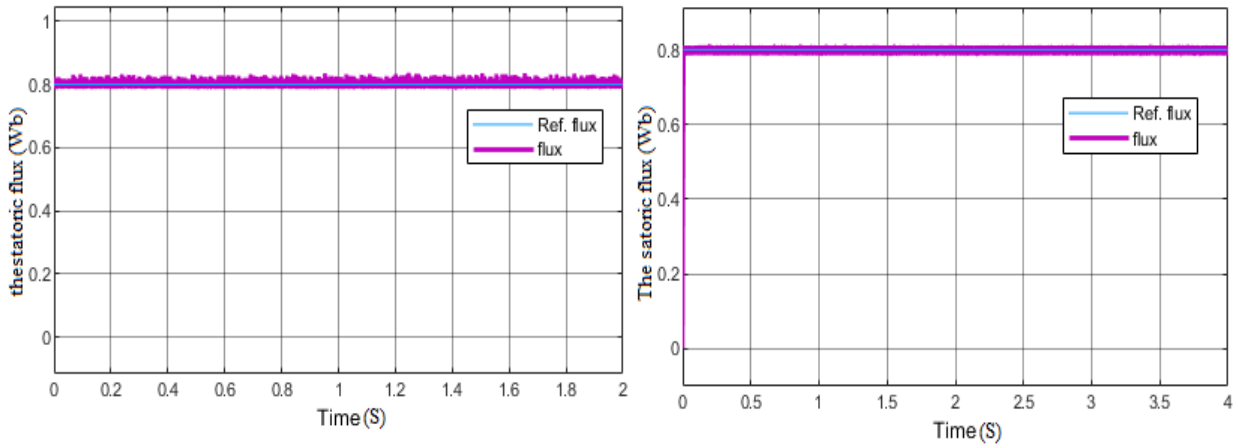

Fig.(3.10) Stator flux magnitude [Wb].

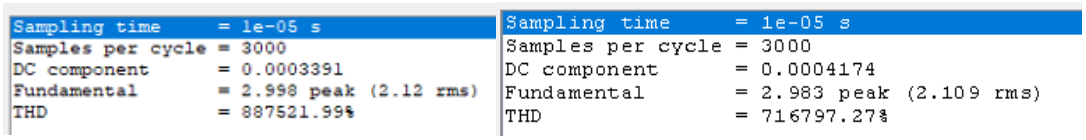

a) b)

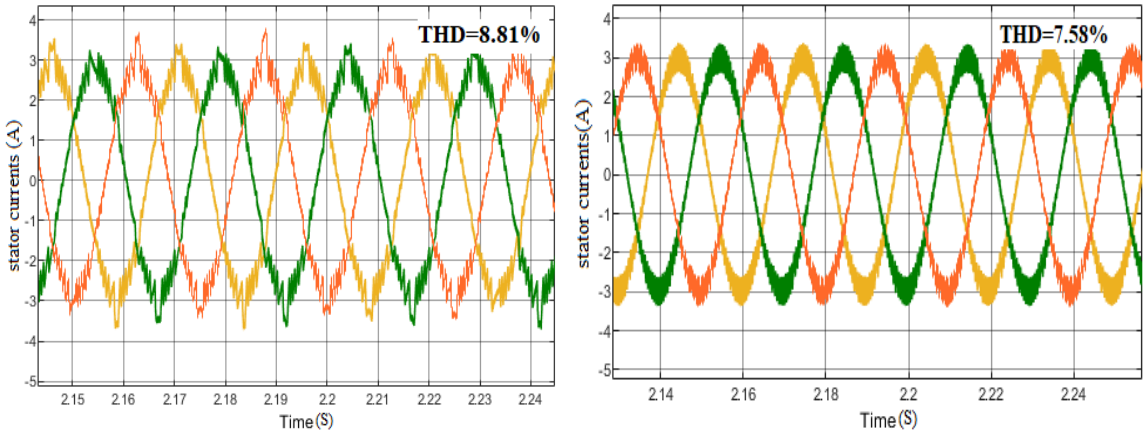

Fig.(3.11) Stator phase currents i_{sa} i_{sb},i_{sc}

The current drawn by the motor is shown in Figure (3.11) (a and b) for the use of the two strategies proposed in this work, where the current takes a sinusoidal shape with ripples. The current value is largely related to the system and the torque value. Furthermore, it can be seen that the current ripples are greater in the case of a conventional DTC control (6 sector) compared to a (12sector) DTC control, where the THD value of the current is low in the case of a 12

sector DTC control (THD=7.58%) compared to a conventional control (THD=8.81%), which is desirable.

a) b)

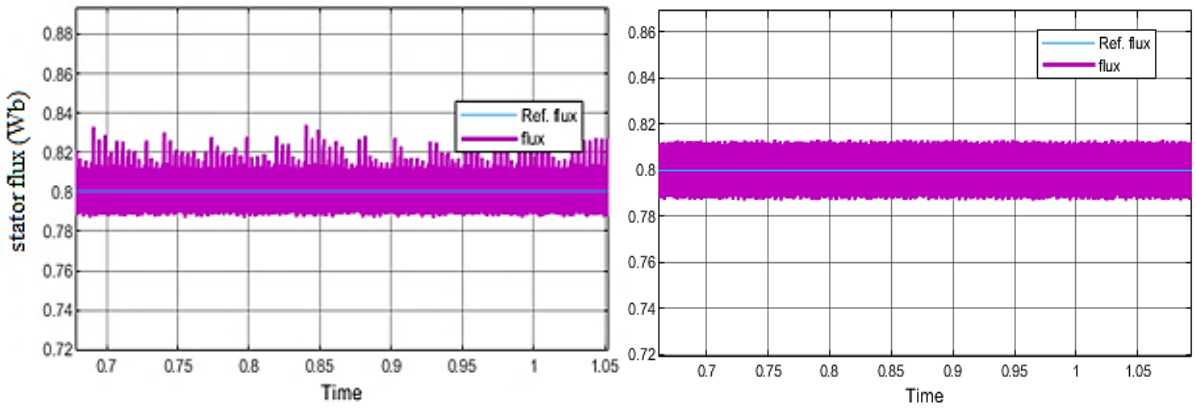

Fig (3.12): ZOOM in stator flux

The displayed simulation results above (FigsIII.8,9,10,11,12) show the starting up and the steady states with no load application for the DTC controlled induction motor. Fig(3.8) illustrates the comparison between speed responses of 6 and 12 sectors according to the speed reference step of 1000 rpm . The figure shows that both techniques show good dynamic at starting up. We can notice that the speed respond quickly in 12 sector better then 6.

Also the real speed follows it reference value same as the torque ,12 sector DTC in improving torque quality and the flux.

The motor flux controlled by both the conventional DTC and 12-sector DTC controls is shown in Figure (3.10), where the stator flux takes a constant value (0.8 wb) equal to the reference value throughout the simulation period with ripples for both drives. The stator flux value is not affected by the torque. Furthermore, the stator flux has a very fast time response, it is noted that the ripples are greater in the case of 6 dtc control compared to the 12 segment DTC control (Figure III.12).

3.10.2 with load application:

This section presents the starting up state of the induction motor according to speed step reference of 1000 rpm. Then, a load of 5N.m at t=3.5s is introduced. Figs (3 .13,14,15,16,17) show respectively rotor speed, torque, stator phase current I_{sa} , stator flux,. The figures are specified: (a) for DTC 6 sector, and (b) for 12 sector.

a) b)

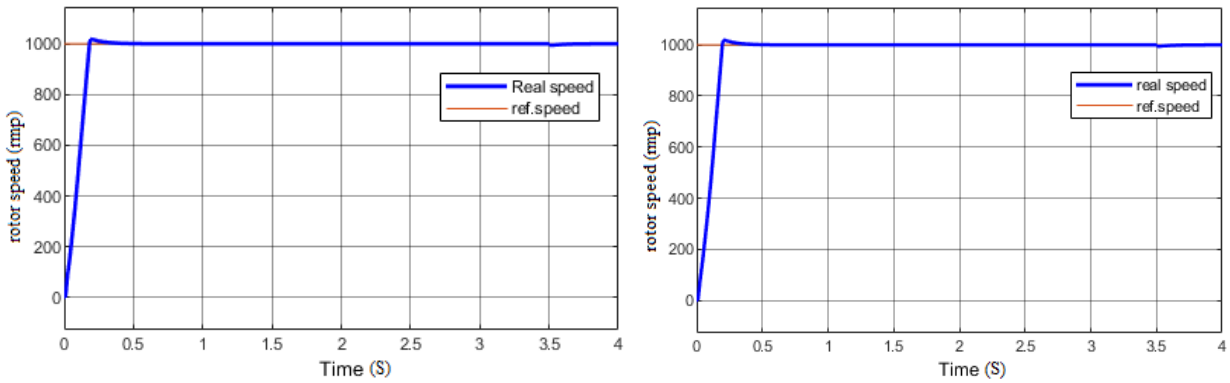

Fig(3.13) Rotor speed response at the starting up and steady states with load application.

a) b)

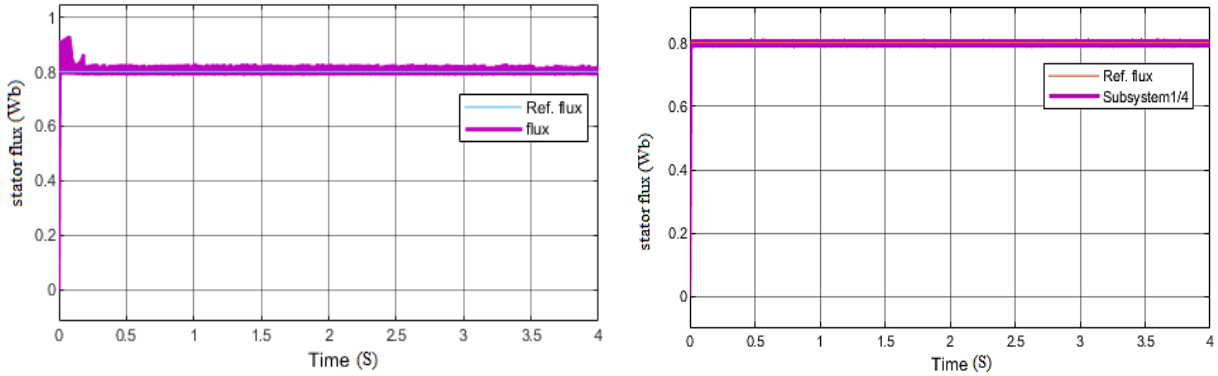

Fig.(3.14) Stator flux magnitude [Wb]

a) b)

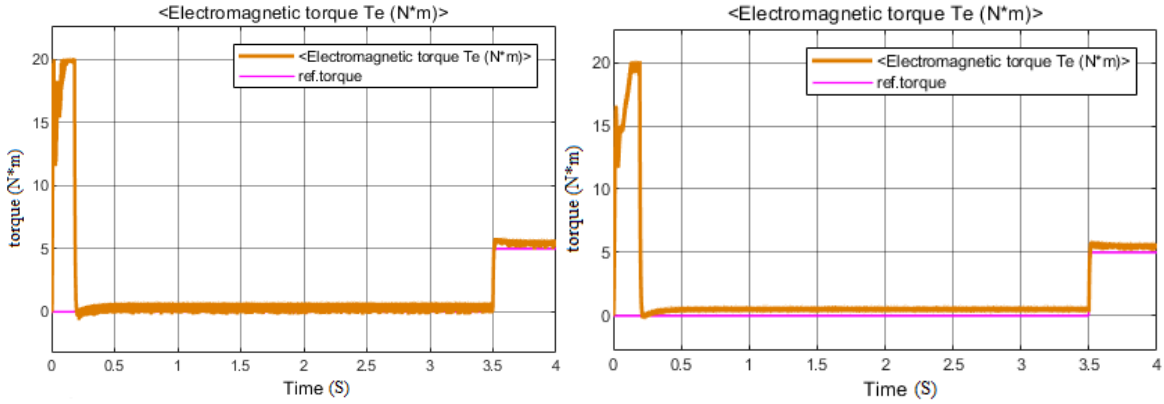

Fig(3.15) Electromagnetic torque with no load application of 5 N.m at 3.5s .

a) b)

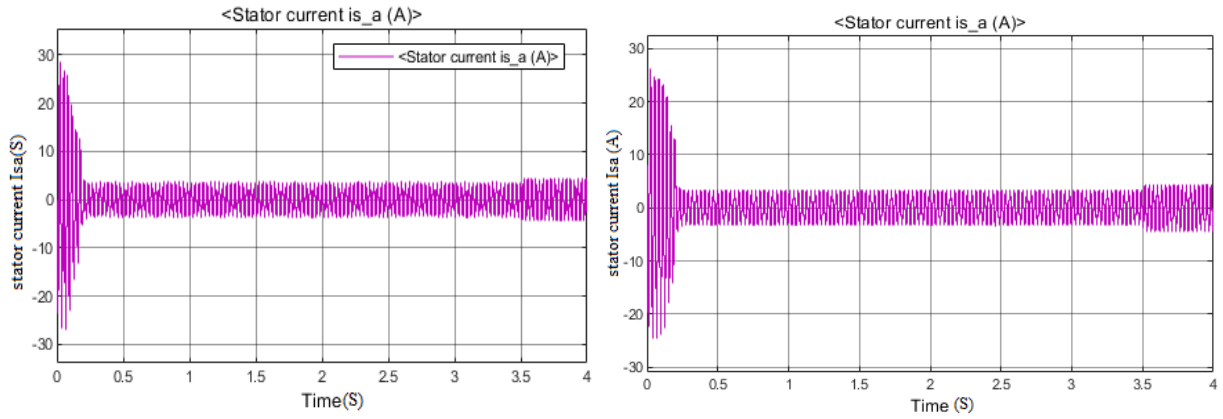

Fig(3.16) Stator phase current i_{sa}.

a) b)

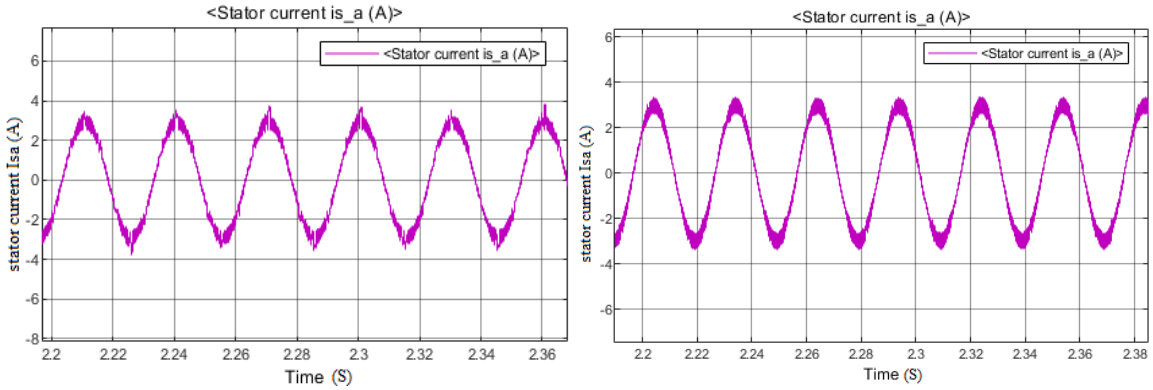

Fig(3.17) ZOOM of stator phase current isa.

The comparative analysis between 6 sectors and 12 sectors demonstrates clear performance improvements when increasing the number of sectors. Starting with the rotor speed response (Fig. 3.13), the system employing 6 sectors shows acceptable behavior during startup and steady state; however, minor overshoots and small oscillations are observed during

transients, under load application, the 12sector DTC exhibits a smoother and faster response, with reduced speed ripple and quicker stabilization after load disturbances. This indicates an enhanced dynamic performance and better tracking of the reference speed.

In terms of stator flux behavior (Fig. 3.14), the 6 sector method results in slight flux oscillations during the transient period, which may affect the precision of torque generation. However, when switching to 12 sectors, the stator flux magnitude remains remarkably stable throughout the operation. The ripple is diminished, confirming that the increase in sector resolution enhances flux control accuracy.

The improvements are even more pronounced in the electromagnetic torque response

(Fig. 3.15). With 6 sectors, the torque exhibits visible ripples and abrupt changes, especially after the load is applied at 3.5 seconds. These fluctuations can lead to mechanical vibrations and reduced control precision. Conversely, the 12 sector DTC delivers a much smoother torque profile, with minimized ripple and a more controlled response during load variation. This smoother transition confirms the superior performance of the 12 sector configuration in maintaining torque stability under dynamic conditions.

the use of 12 sectors in DTC results in a substantial enhancement in control quality. The system achieves better speed regulation, reduced stator flux and torque ripples, and improved stability during load transients. These findings underline the effectiveness of increasing the number of sectors in DTC to achieve higher drive system performance and robustness,the same as the stator current in Fig(III.16,17) it takes sinusoidal form but the Shattering in 6 sector current is Higher then the 12 sector current and in time 3.5s react to the load application ,it began bigger because of the load consume more energy .

3.10.3 Rotation sense's reversing:

a) b)

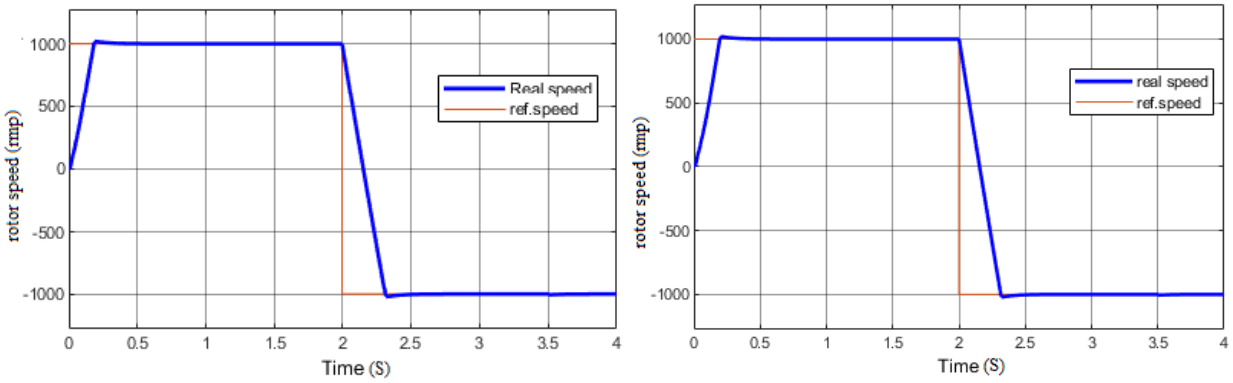

Fig(3.18) Rotation sense's reversing: rotor speed (1000rpm ,–1000rpm)

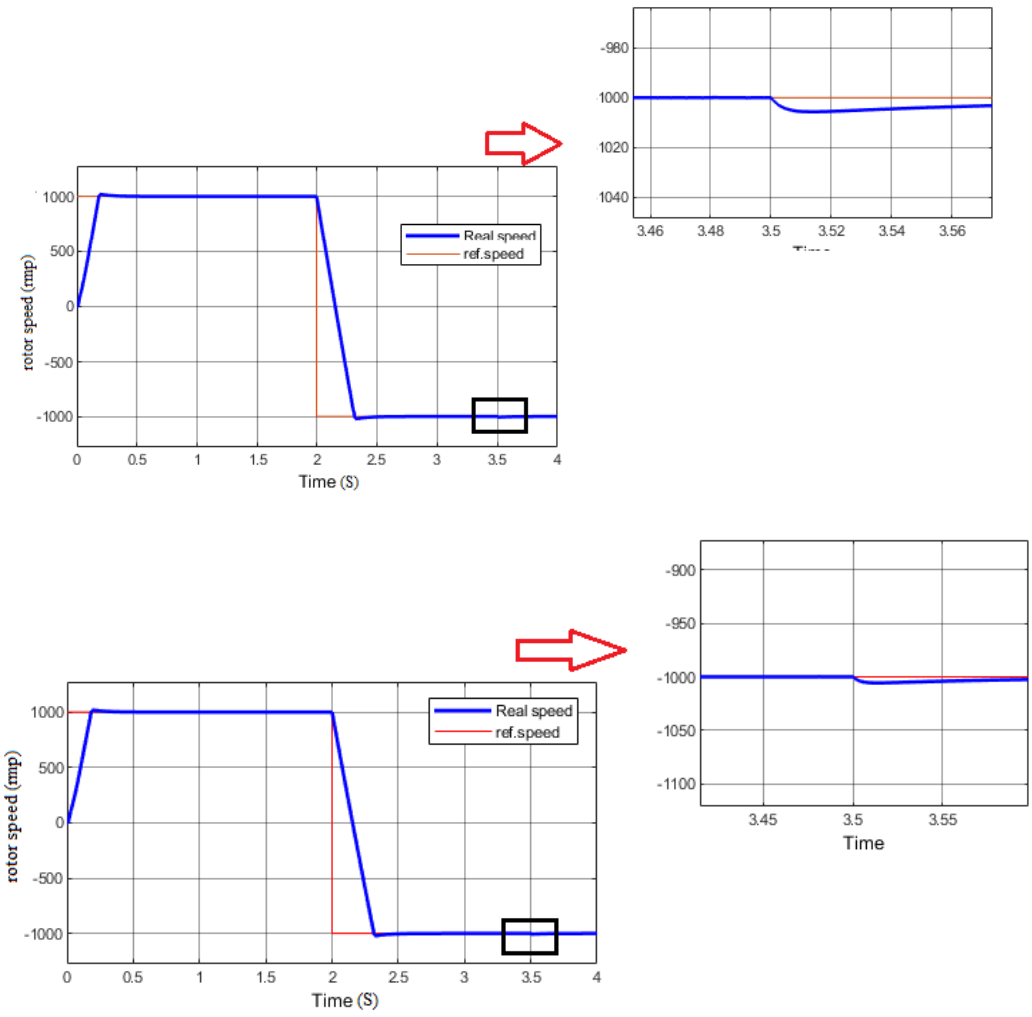

Fig(3.19) Rotation sense's reversing: ZOOM in rotor speed the 6 and 12 (1000rpm ,–1000rpm)

a) b)

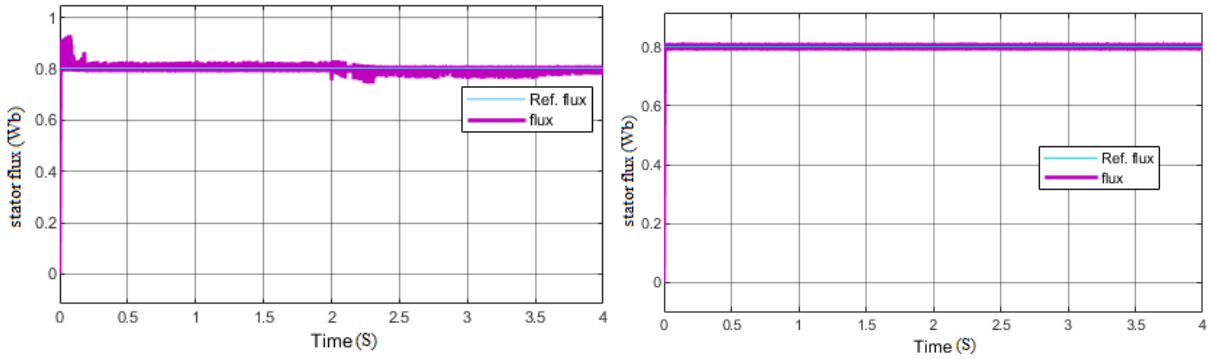

Fig.(3.20) Rotation sense reversing: stator flux (Wb).

a) b)

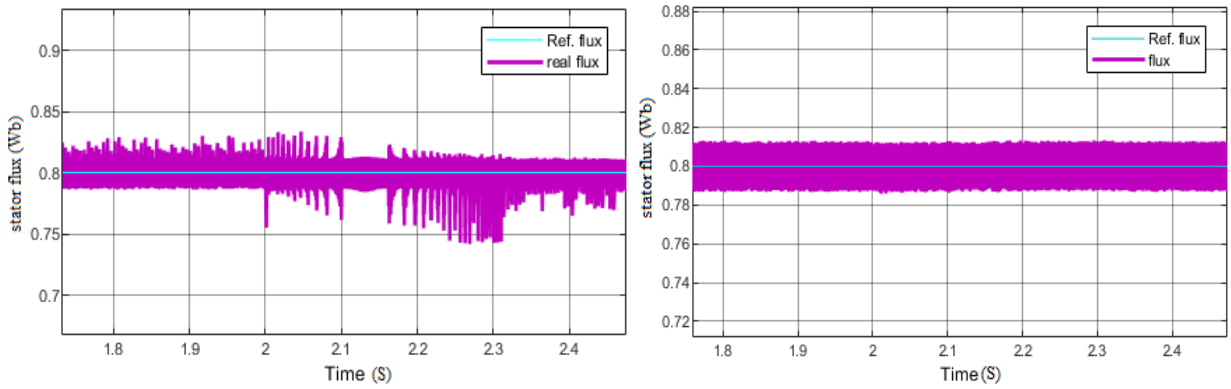

Fig(3.21):ZOOM in stator phase flux (Wb)

a) b)

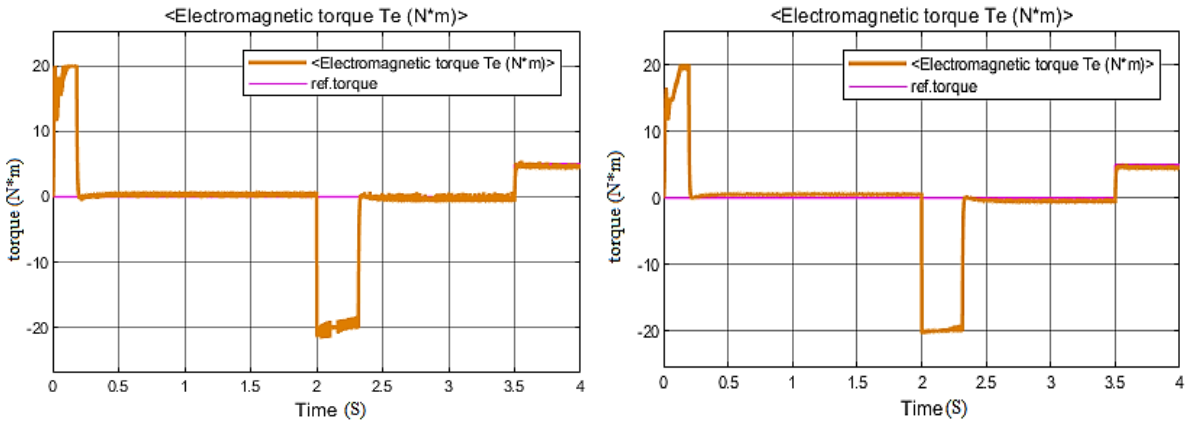

Fig(3.22):Rotation sense reversing : Electromagentic torque [N.m].

a) b)

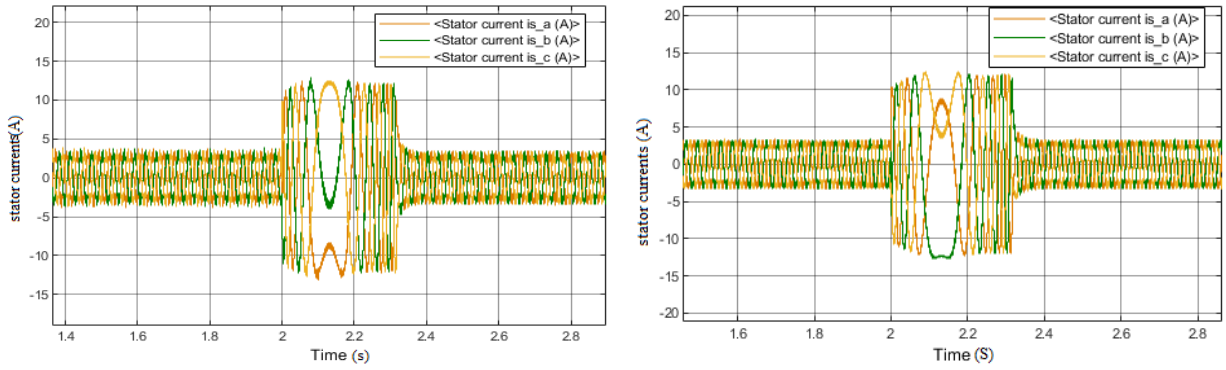

Fig(3.23) Rotation sense reversing: Stator phase currents [A].

a) b)

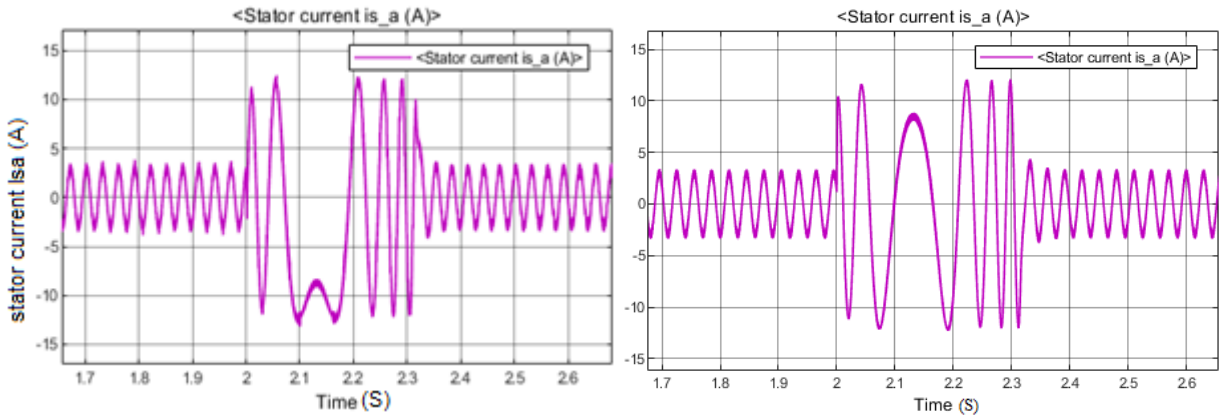

Fig(3.24) Rotation sense reversing: Stator phase current I_{sa} [A].

A speed reversal from a positive to a negative value (1000 rpm to –1000 rpm) is performed in Figures (3.18 to 24) to demonstrate the ability of DTC to operate effectively across a wide range of speeds. During the reversal phase, the speed controller behaves similarly to the startup phase, driving the system to its physical limits. This is particularly evident in the torque response shown in Figure (3.22). The speed and torque curves in Figures (3.18) and (3.22) exhibit strong dynamic performance and accurate reference tracking in both transient and steady state conditions., the 12 DTC method delivers improved dynamic behavior with noticeably reduced torque ripples. Figures (3.23) and (3.24) illustrate the reversal of stator currents and Stator phase current I_{sa} for both control techniques, showing well formed sinusoidal waveforms and a lower harmonic content with 12 DTC.

The stator flux response different between the two control strategies. In the case of the 6 DTC (Figure a.3.20) and zoomed in (3.21) the stator flux exhibits a noticeable ripple around its reference value, with noticeable fluctuations, especially around the two second mark during reversal. This behavior indicates less precise flux control during dynamic transitions, the 12 DTC (Figure b.3.20) exhibits a smoother flux response, with minimal ripples and improved tracking of the reference value, even during reversal. This reflects more precise and stable flux regulation, with the 12 dtc better dynamic performance than the 6 sector, the torque experiences a sharp overshoot in, (Figure a) and significant oscillations during the reversal phase. The ripple is quite pronounced, particularly during dynamic transitions, and the system exhibits a longer settling time after the reversal In the 6 sector DTC case.

The 12 sector DTC (Figure b) shows a much smoother torque reversal, with reduced ripple and quicker stabilization to the new torque reference. This indicates a superior dynamic response and places less mechanical stress on the motor, making the 12 sector approach more effective for high performance applications.

3.10.4 Speed variations:

a. Without load

we did change in rotor speed from 1000 to1300 rmp without load and this the results with time=2s, a) is 6 sector and b)12 sector

the figures (3.25to 28) we have the rotor speed, Electromagnetic torque, stator flux, and currents.

a) b)

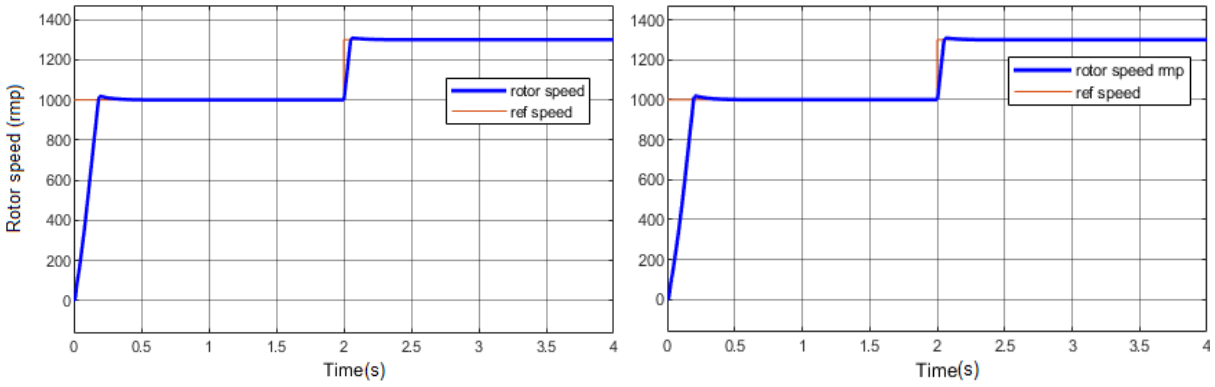

Fig(3.25)Speed variation without load: rotor speed (1000rpm to1300rpm)

When comparing the speed response in both cases, we observe that both the 6 sector (a) and 12 sector (b) configurations effectively follow the reference speed during the variation from 1000 rpm to 1300 rpm, the 12 sector DTC (b) exhibits a slightly smoother transition with reduced ripple and better accuracy. the voltage vector space in the 12 sector scheme allows for more precise voltage vector selection, improving dynamic response.

a) b)

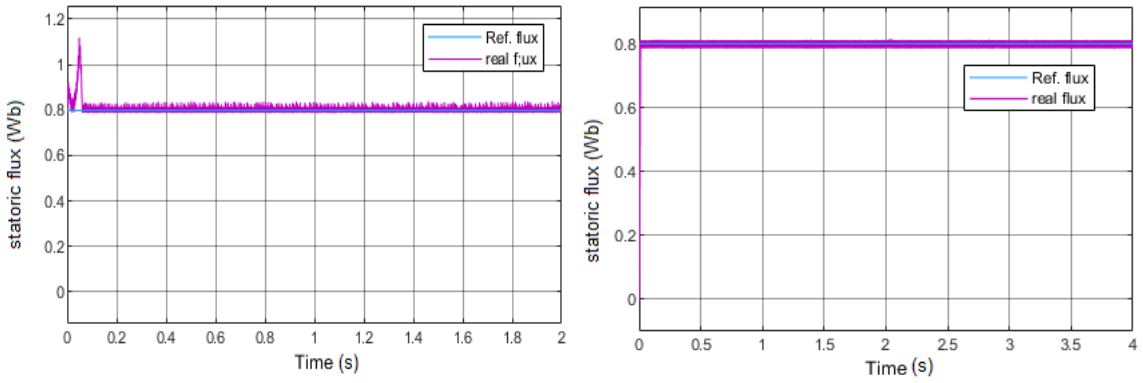

Fig (3.26) stator phase flux (Wb)

The stator flux components in both cases maintain a stable trajectory close to the reference values. In the 6 sector case (a), some small oscillations may appear in the flux waveform due to the coarser resolution of vector selection. On the other hand, the 12 sector approach (b) shows a smoother and more continuous flux path, thanks to the increased number of available control vectors. This leads to reduced flux ripple and improved electromagnetic torque control.

a) b)

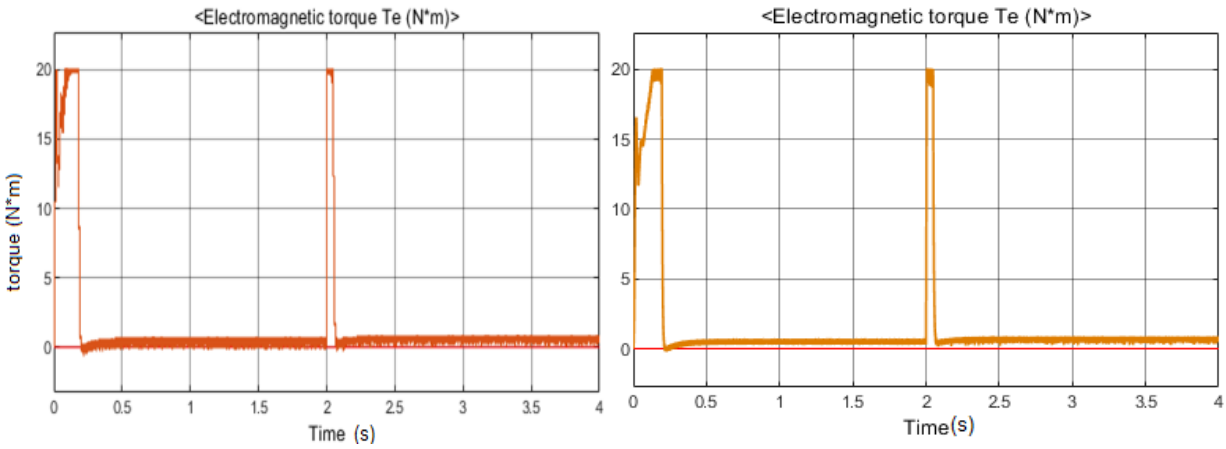

Fig(3.27): Electromagentic torque [N.m].

a) b)

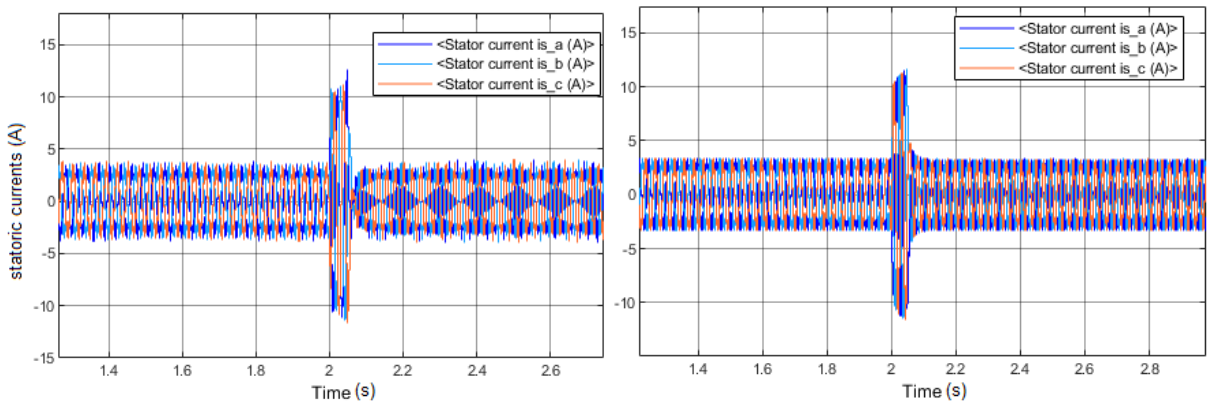

Fig(3.28)Stator phase current Isa I_{sb} I_{sc} [A].

The 12 sector approach provides smoother torque transitions and reduced ripple, which is crucial for enhancing machine lifetime and improving performance in applications requiring precise torque control. The peak torque values remain similar, but the smoothness in (b) is better then (a).

The second set of plots (Fig 3.28) displays the stator phase currents. In the 6 sector (a), the currents show visible oscillations and distortions during transient events, which can contribute to undesirable harmonics put stress on the motor. the 12 sector control (b) results current waveforms, even during speed variation the reflects better control of the stator flux vector and demonstrates the effectiveness of the increased sector resolution in waveform quality.

b.With load:

same conditions with load at time t=3.5s and speed variation at 2, a) is 6 sector and b)12 sector

a) b)

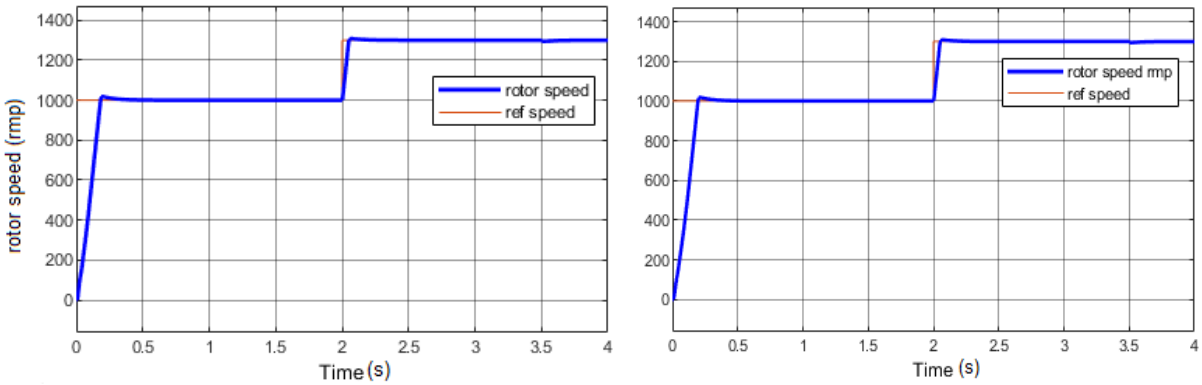

Fig(3.28)Speed variation with load: rotor speed (1000rpm to1300rpm)

a) b)

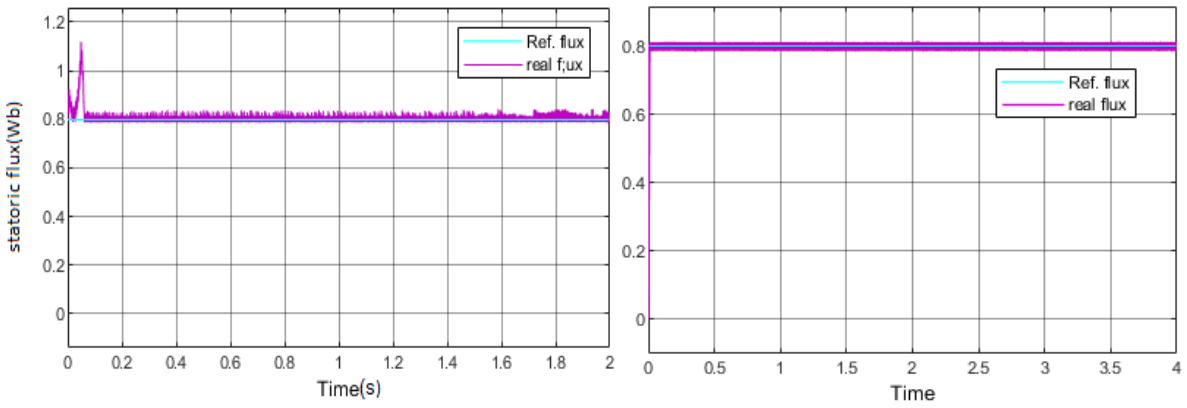

Fig (3.29) stator phase flux (Wb)

a) b)

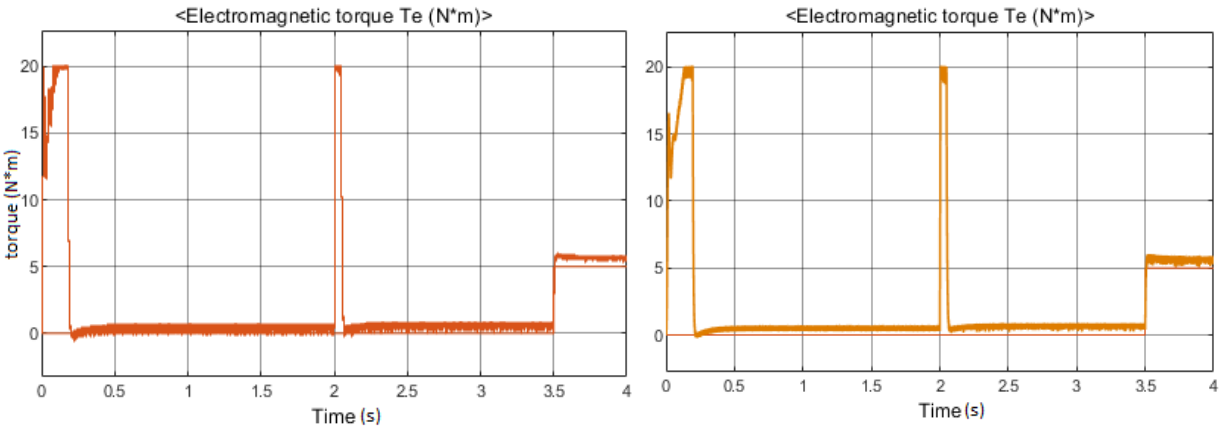

Fig(3.30): Electromagentic torque [N.m].

a) b)

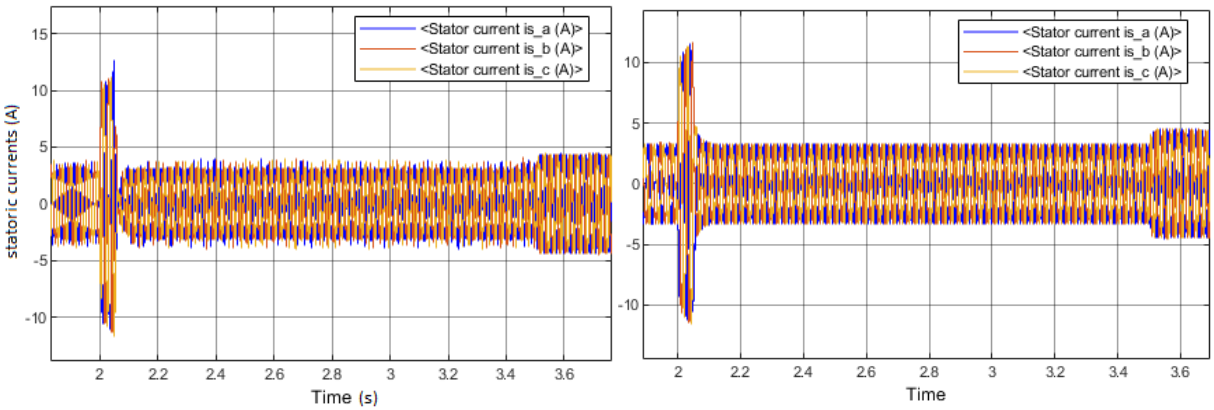

Fig (3.31) Stator phase current Isa I_{sb} I_{sc} [A].

When a load is applied, the torque response becomes more important. In the 6 sector (a), the torque shows noticeable ripples and is less stable, especially during speed changes. The 12 sector version (b) performs better, with smoother torque and fewer fluctuations.

Looking at the stator currents when we applied load at time 3.5s the motor start consuming more energy and the current increase, the 6 sector method shows more distortion, particularly during transients. In contrast, the 12 sector setup results in cleaner and more balanced current waveforms, showing better control over the motor.

the 12 sector DTC offers better performance under load. It gives finer control, smoother torque, and cleaner currents, making it more suitable for situations where precision and stability are important.

3.11 Conclusion

This chapter focused on applying two types of Direct Torque Control (classic DTC and 12 sector DTC) to an induction motor fed by two-level inverters. While DTC offers robust and dynamic performance, it struggles with uncontrolled switching frequency. Simulation results show that 12 sector DTC provides better static and dynamic performance than the classic version, with improved speed tracking and torque flux decoupling. It also reduces torque and flux ripples. However, torque ripple remains an issue that needs addressing to enhance system efficiency.
The following chapter will be dedicated to Direct Torque Control (DTC) experimental validation with comparison between 6 sector and 12.

Chapter Four:
Experimental validation

1.1.Introduction

In this study, we took a close look at two ways of doing Direct Torque Control, or DTC the 6 sector and the 12 sector methods. Now, both of these have their downsides. You can see things like the switching frequency jumping around, the torque and magnetic flux wobbling a bit, and the current acting a little unpredictable sometimes, whether things are changing or staying steady, However, we noticed that these problems are definitely less of an issue with the 12-sector DTC compared to the standard 6-sector one. As we showed you back in Chapter 3, this leads to better overall performance [23].

So, the first part of this chapter is all about the experimental setup we used. Then, in the second part, we really wanted to see if our simulation results held up in the real world. Our goal was to confirm that the 12 sector DTC really does have those performance advantages we saw in the simulations. To do this, we ran a bunch of experiments, specifically focusing on how much the torque and flux were rippling just like we did in the simulation phase.

We actually implemented all the control brains using Matlab, Simulink, and the dSPACE 1104 system. It's also worth mentioning that all this testing and validation happened at the Electrical Engineering Lab in Biskra (that's the LGEB), using the test bench we set up there [23].

4.2. Representation of experimental material

This chapter presents the development of an experimental platform designed to validate the simulation results. The setup features a 3 kW squirrel cage induction motor (IM) powered by a voltage inverter. Doubly fed induction machine (DFIM), operating as a generator, serves as the load and is mechanically coupled to the IM shaft. Two rheostats are connected in series with the (DFIM) armature to apply a variable load to the motor. Rotor position is detected using a 1024 pulse incremental encoder, and phase currents are measured via Hall effect sensors. The control algorithm is implemented on a dSPACE DS1104 board, using Control Desk software in conjunction with MATLAB/Simulink. This experimental platform enables real-time testing and evaluation of the control strategy under practical operating conditions. The IM parameters, determined through standard testing methods, are provided in Appendix A. The test bench setup developed at the LGEB laboratory in Biskra [23].

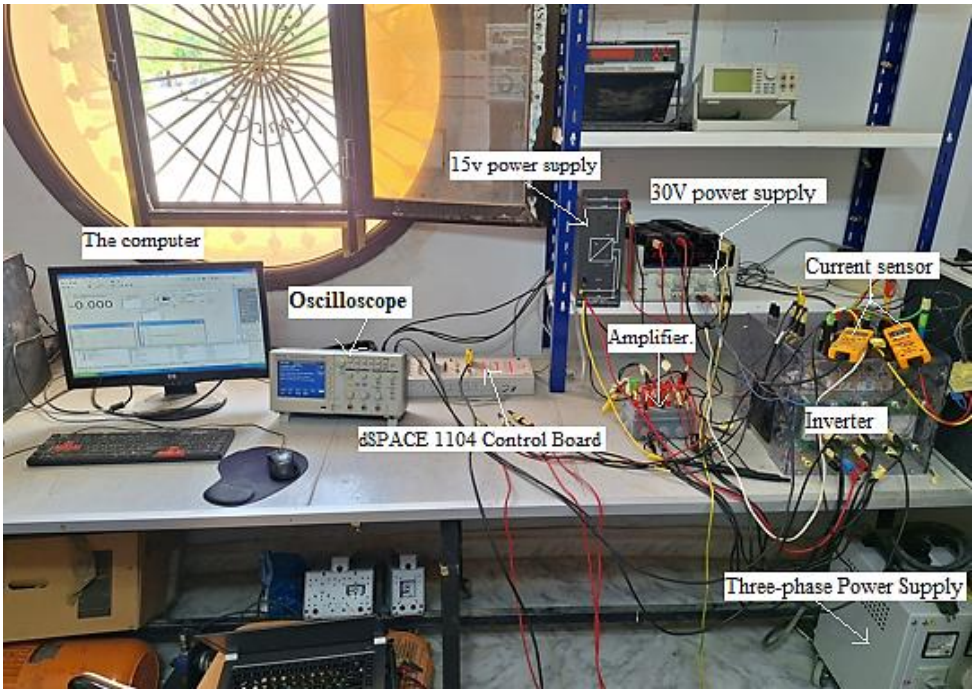

Fig(4.1):Im experimental platform (Lab. LGEB)

4.3Power Part:

- **Electrical Source:**

a) Three-phase Power Supply:

This supplies the motor with power via an inverter. It is used to modify the effective value of the phase to phase voltage [23].

Fig(4.2) Three-phase Power Supply

b) 30V power supply:

the 30-volt power supply used in the experimental setup.

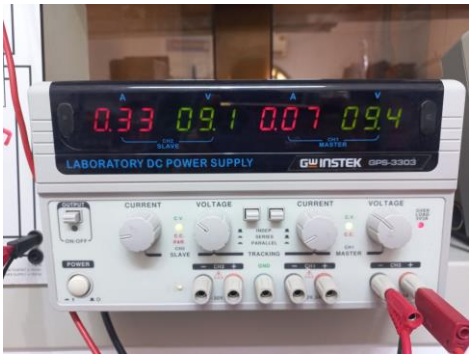

Fig(4.3):30V power supply

C)Electric machine :

This work is based on the use of a 3 kW didactic squirrel-cage induction motor (a), which is mechanically coupled to a 4 kW doubly fed induction motor (DFIM)acting as to apply the load (b)[23].

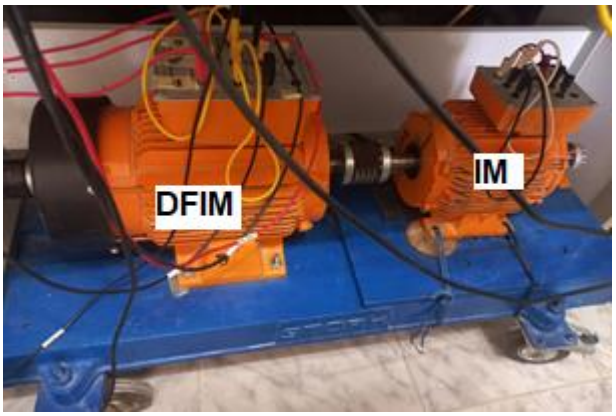

Fig(4.4) IM and DFIM used as load

e) Converter:

The speed control device serves as the power source for operating the electric machine. Our design requires this power converter to provide open access for controlling the three IGBT bridge arms. It is feasible to design the inverter using commercially available power modules intended for industrial applications. In our case, a two level 20 kVA inverter using IGBTs is required [23].

4.4 Control part:

a) signal conditioning circuit:

It is used to amplify and adapt the control signals generated by the DS1104 board to drive the IGBT power transistors. Its main function is to increase the voltage level from 5V to 15V [23].

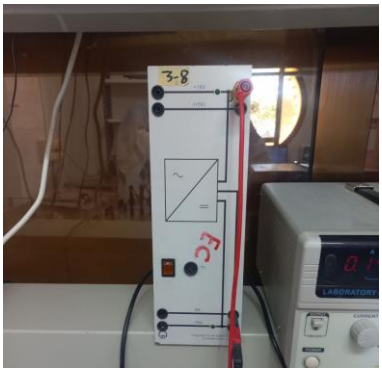

Fig (4.5)signal conditioning circuit

b)Speed sensor:

In our practical tests, a 1024 pulse incremental encoder was used to measure the speed[23].

c)dSpace1104 Control Board:

his card is operated by Control Desk and Matlab/Simulink software.

d)current sensor:

To measure the stator currents, we used two Fluke clamp type current probes. These sensors operate based on the Hall effect, detecting the magnetic fields generated by the electric current. Powered by a 9V supply, they provide an accurate representation of the stator current. Each sensor has a maximum measurement capacity of 20 A and a conversion ratio of 100 mV[23].

Fig(4.6): current sensor:

e)Oscilloscope:

To obtain the experimental results, it is necessary to use specialized, high-quality equipment.

the 4 channel Tektronix oscilloscope used in this work to capture and extract the experimental data [23].

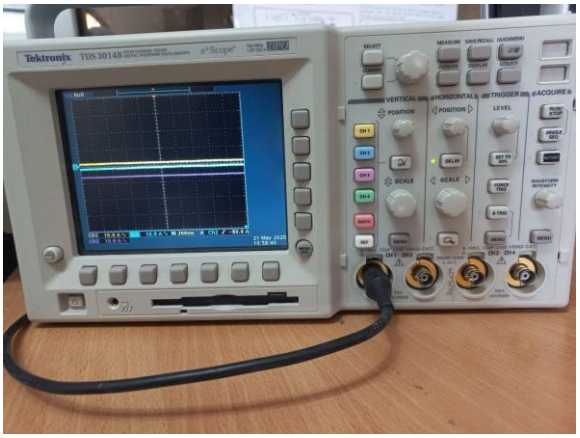

Fig(4.7) : Oscilloscope Tektronix 4 voies.

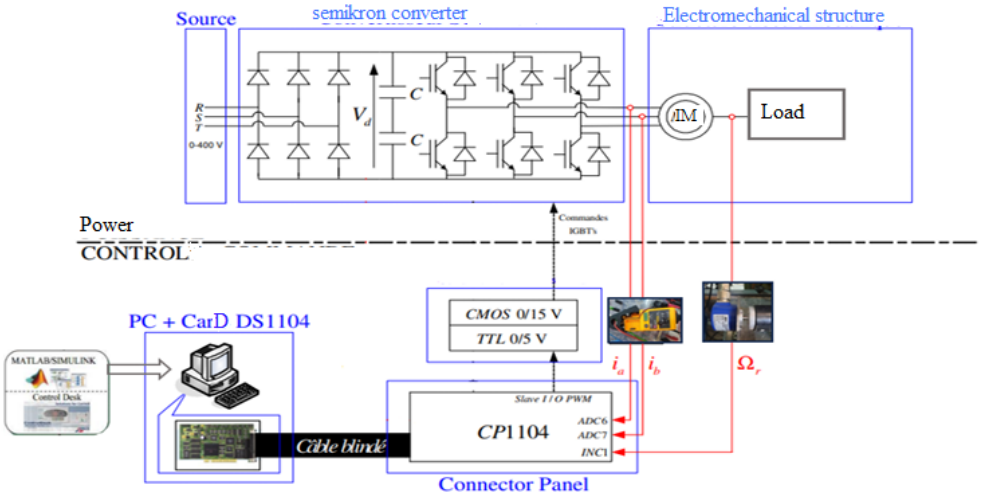

Figure(4.8)Block diagram of the experimental platform.

4.5 Software Part

4.5.1 Working with RTI

To connect your model to a dSPACE I/O board, you simply need to drag and drop the appropriate I/O modules from the RTI block library into your Simulink model and link them to the corresponding blocks. All configuration settings, including parameter adjustments, can be accessed by clicking on the specific blocks. Simulink Coder (formerly Real Time Workshop)

automatically generates the necessary code, while RTI provides the I/O interface blocks that enable integration of dSPACE hardware into your Simulink environment. This setup prepares your model for real time execution. Once configured, the model is automatically compiled, downloaded, and executed on the real time hardware without requiring any manual programming. Additionally, RTI assists during the configuration process by performing consistency checks to identify and correct potential issues before or during compilation [28].

4.5.2Control Desk:

Control Desk serves as a simulation platform comparable to MATLAB. It offers a user friendly interface for real time monitoring and adjustment of variables from the Simulink model while the system is in operation. Unlike RTI, which requires recompilation of the generated source code for every change, Control Desk bypasses this step, allowing quicker and more efficient modifications. Moreover, it supports the recording of signals corresponding to the system's electrical variables, which can be exported for further analysis in MATLAB [23].

4.6 Description of the dSPACE 1104 Board:

As you can see in Figure 5.13, we identified the harmonic currents using the dSPACE digital system specifically, the DS1104 prototyping board.This board was hooked up to our MATLAB/Simulink setup through the Real Time Interface (RTI) block. The DS1104 system itself is made up of a few key parts [25]:

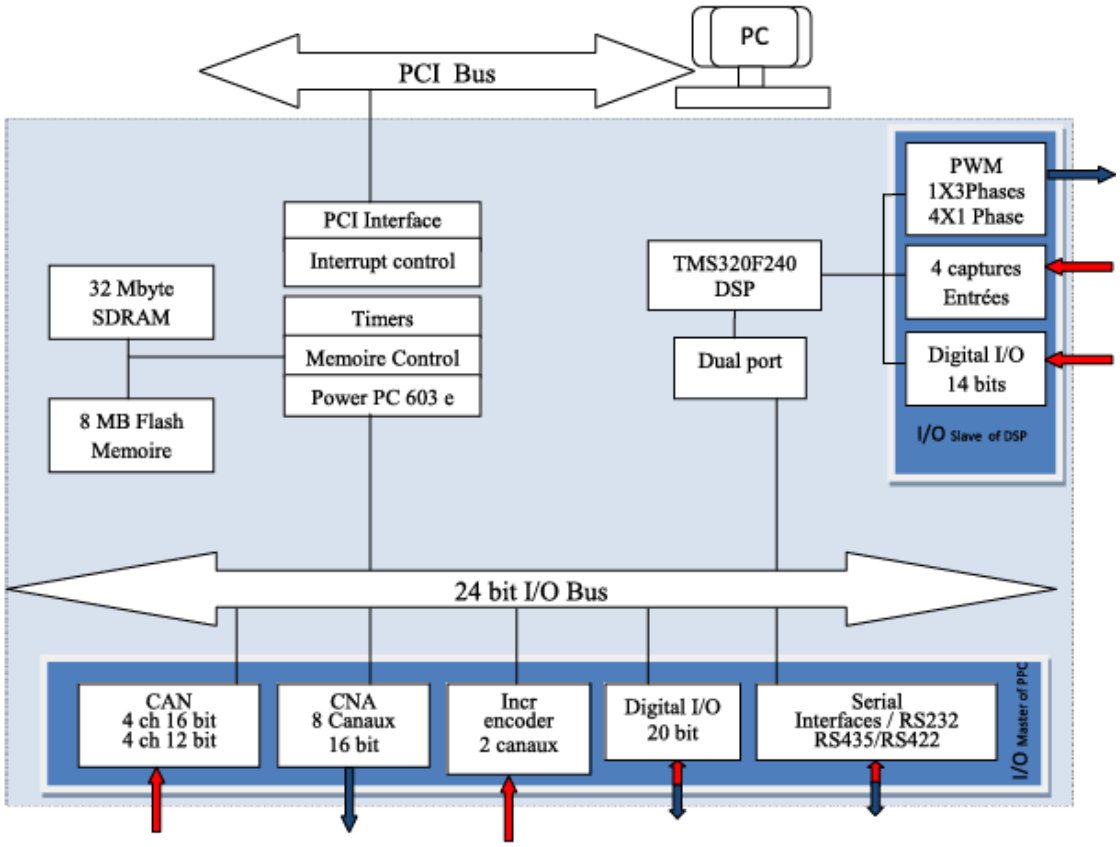

Figure (4.9) Composition of the DS1104 card.

1. The DS1104 motherboard, installed in the computer, which manages the overall operation of the system and runs the main program.
2. 20-bit digital input/output interfaces.
3. A DSP card from Texas Instruments, model TMS320F240.
4. Four single-phase PWM outputs and one three-phase PWM output.
5. Two incremental encoders.
6. 14 bit analog inputs.
7. A multi-input, multi output connection panel that ensures the interface between the various sensor outputs and the DS1104 card (installed in the PC)[25].

The panel includes the following components:

- Two sets of four BNC input connectors connected to the Analog-to-Digital Conversion (ADC) board. It is important to note that the input signals must be scaled by a factor of 10, as the ADC hardware automatically divides the input values by 10.
- Two sets of four BNC output connectors linked to the Digital-to-Analog Conversion (DAC) board. Similarly, the output signals must be scaled down by a factor of 10, since the DAC hardware multiplies the output values by 10.
- The output voltage range is ±10V.[25]

Current measurements are performed using LEM sensors, which have a transmittance of 100 mV/A.

A key advantage of this controller lies in its ability, through appropriate software, to automatically convert control models developed in Simulink into assembly code, compile them, and load them into the DSP. This enables control strategies to be first tested in simulation using Simulink and then automatically translated into executable code for the controller[25].

Another notable benefit of this control system is the experimentation software, Control Desk**,** which allows for real-time visualization, data logging of various system quantities, and on-the-fly modification of control parameters[25].

4.7. Experimental Results:

To experimentally validate the results obtained in the previous simulation chapters, practical tests were carried out. Signals were recorded under different operating conditions, including no load tests with speed variation and load tests. These tests were conducted for both control strategies conventional DTC and 12 sector DTC within a comparative study. The figures are labeled as follows: (a) for conventional DTC and (b) for 12 sector DTC.

4.8.1No Load With Speed Variation:

In this test, the performance of both control strategies was examined and verified during a no load speed change from 1000 rpm to 1300 rpm. The results of this experiment are shown in Figures (4.10 to13) For this test, the scaling and gain settings were adjusted to prevent saturation of the dSPACE system: for torque, a scale of 500 mV with a gain of 0.01 was used; for speed, a scale of 500 mV with a gain of 0.0001; and for flux, a scale of 400 mV with a gain of 0.1,

a)6 sector DTC, b)12 sector DTC.

Figure (4.4) illustrates both the electromagnetic torque and the motor speed. It is clearly visible that the PI speed controller successfully tracks the reference in both control strategies (with 1 division = 500 rpm). Regarding the torque, it follows the reference value throughout the test, though a transient effect is observed when the speed changes from 1000 rpm to 1300 rpm. During this transition, the torque briefly spikes to its maximum before gradually decreasing. Torque ripple is present in both cases, but it is noticeably reduced when using the 12sector DTC control method.

a) b)

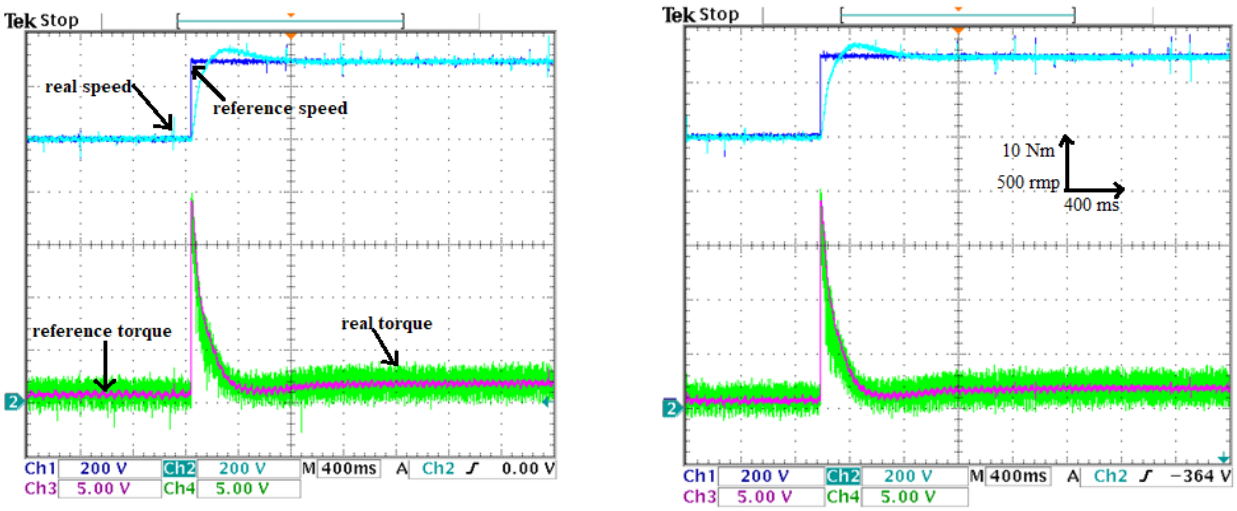

Ch1: reference speed, Ch2: actual speed, Ch3: reference torque, Ch4: actual torque.

Figure (4.10): Electromagnetic Torque and Speed (No Load and With Speed Variation).

a) b)

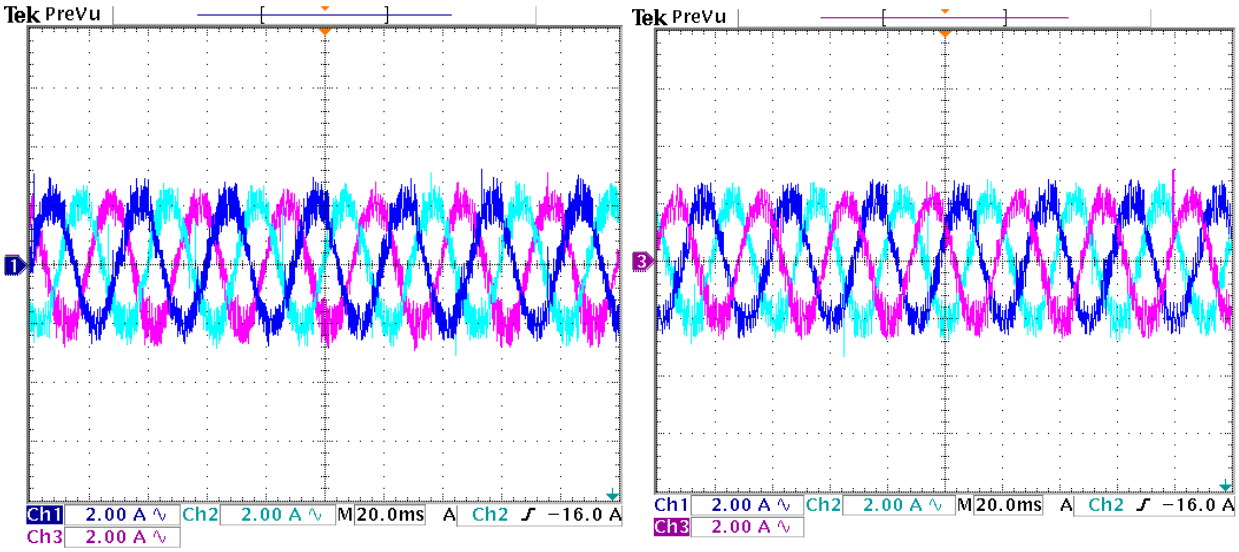

6 sector :Ch1,Ch2,Ch3 represent the stator currents $\mathbf{I_{sa}b_c}$.

12 sector :Ch1,Ch2,Ch3 represent the stator currents $\mathbf{I_{sa}b_c}$.

Figure(4.11): Zoom on the Steady-State of Stator Currents.

Figure (4.11) presents a zoomed view of the stator currents drawn by the motor, based on experimental results for both control techniques. It can be observed that the 12 sector DTC produces a more sinusoidal current waveform, regarding torque, this figure(4.10) confirms that torque ripple is more pronounced with conventional DTC compared to the 12 sector DTC. These experimental findings are consistent with the simulation results discussed in Chapter 3.

a) b)

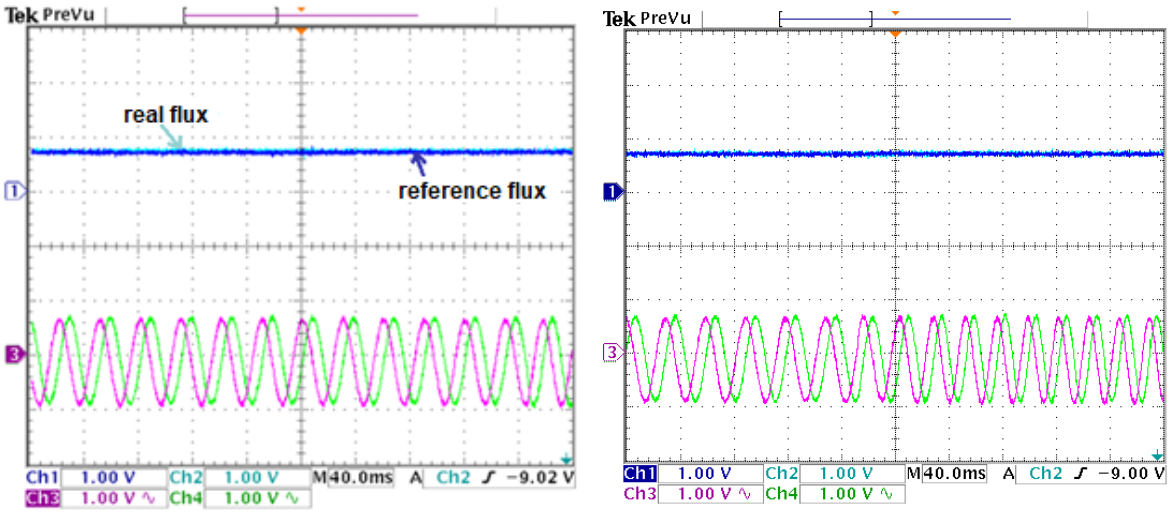

ch1 : reference flux, ch2 :real flux, ch3 et ch4 are the flux components

Fig (4.12): Stator Flux and Its Components (No-Load and With Speed Variation).

The Fig(4.12) It shows the stator flux and its components for both control methods, where the flux maintains a constant value and closely follows the reference with some ripple. This ripple is significantly lower in the case of 12 sector compared to conventional control, the stator flux components exhibit a more sinusoidal waveform under the 12 sector, demonstrating better performance than the classical DTC.

a) b)

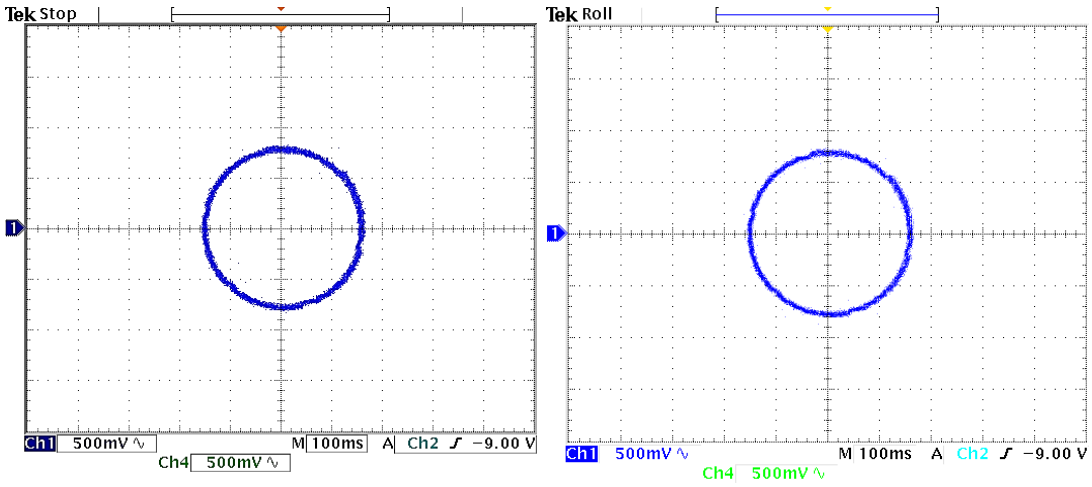

Ch1 :Ψsα, ch2 : Ψsβ

Figure (4.13): Evolution of Stator Flux Components (No Load and With Speed Variation).

Figure (4.13) displays the evolution of the stator flux under no load conditions for both classical and 12 sector DTC control strategies. In both cases, the stator flux forms a circular trajectory. However, it is clearly observed that with the 12 sector DTC, the flux path in the (α, β) plane is more perfectly circular and exhibits significantly fewer ripples. These results reinforce the earlier findings and confirm that the 12 sector method offers improved flux control with reduced ripple compared to the conventional DTC approach.

4.9 With Load test

In this section, we present the load test results obtained on the experimental platform for both control strategies. Figures (4.14 to 17) display the experimental results of the classical DTC and the 12 sector DTC applied to the squirrel-cage induction machine (SCIM) powered by a two-level inverter. The motor is operated at a speed of 1000 rpm. The sampling time is set to Te = 10^{-4} s using the Euler method. The reference stator flux is set to 0.8 Wb.

For this test, the torque measurement was scaled with a 500 mV range and a gain of 0.01, while the speed was scaled with a 500 mV range and a gain of 0.0001. These scale and gain values were

adjusted to prevent dSPACE saturation and to better capture dynamic changes, particularly in terms of speed.

a) b)

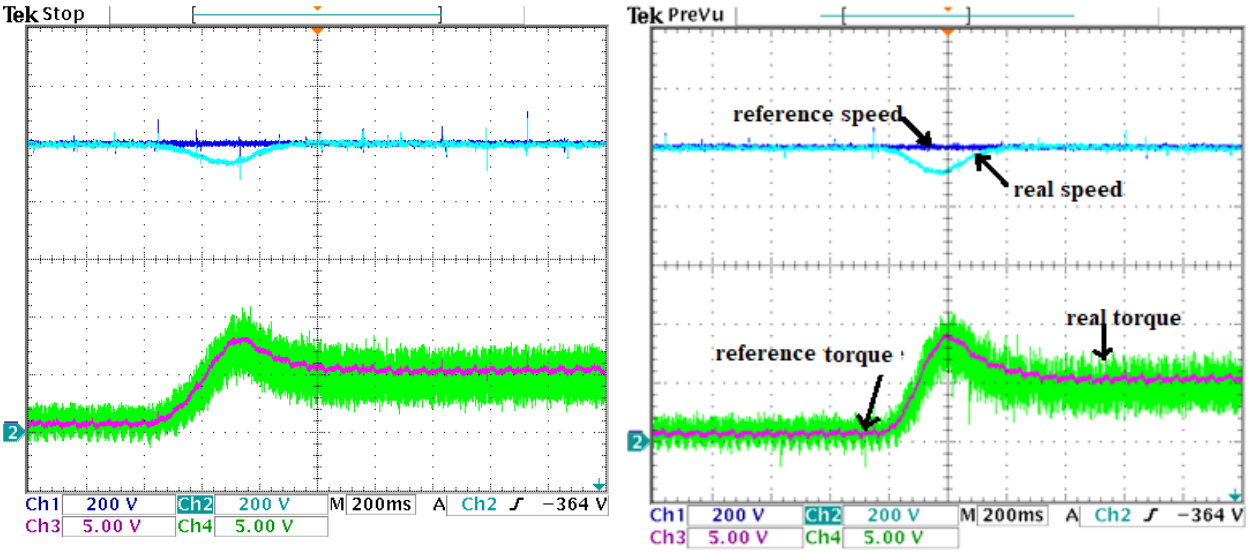

Ch1: reference speed, Ch2: actual speed, Ch3: reference torque, Ch4: actual torque.

Fig (4.14): Electromagnetic Torque and Speed(Speed Variation with Load).

Figure (4.14) shows the motor's rotational speed and electromagnetic torque. As seen in the figure, the speed (1 division = 500 rpm) closely follows the reference, and it is clearly evident that the PI speed controller has no difficulty maintaining the reference for both control strategies. A slight drop in speed occurs at the moment the load is applied. These results strongly confirm the simulation findings and demonstrate the superiority of the 12 sector DTC control compared to the conventional DTC, particularly in terms of reducing torque ripple.

It can be observed from this figure that the motor torque closely follows the reference torque for both proposed control strategies. Additionally, when the load is applied, the electric current increases in magnitude, indicating the system's response to the added mechanical demand.

This increase corresponds to the value of the applied load torque (resistant torque), torque is observed, as shown in Figures (4.14). These ripples are significantly more pronounced with the conventional DTC compared to the 12 sector DTC. The experimental results obtained here are

consistent with those presented in the simulation section, confirming the validity of the earlier findings and highlighting the superior performance of the 12 sector DTC strategy.

a) b)

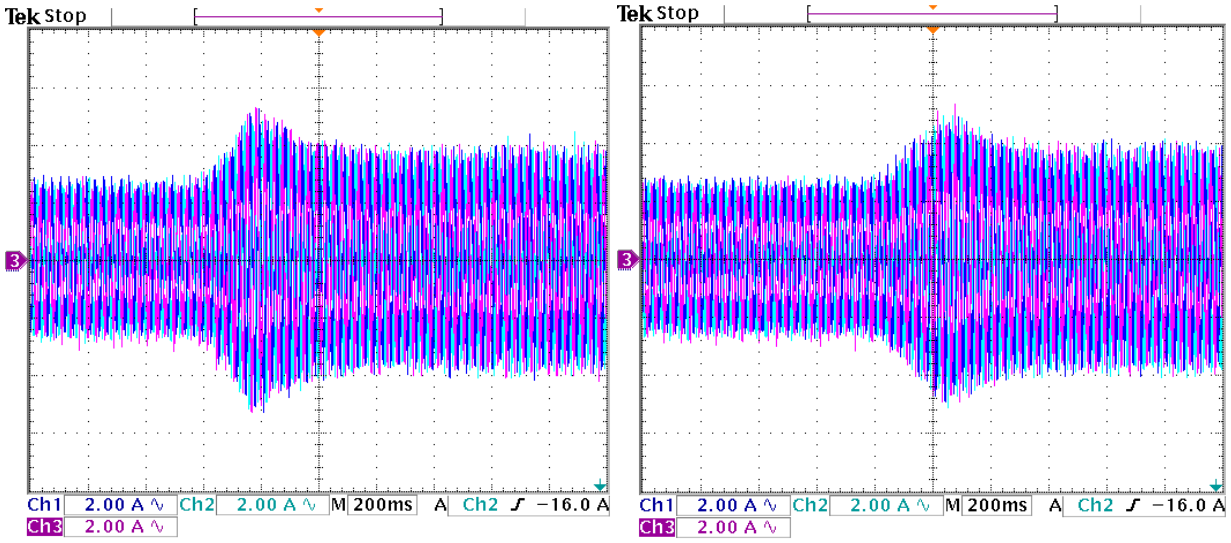

Figure (4.15): Stator Current Isa I_{sb} I_{sc} (Under Load Conditions).

Figure (4.15) the stator current waveforms (I_{sa}, I_{sb}, I_{sc}) under load conditions for two different Direct Torque Control (DTC) strategies. the classical 6 sector and the improved 12 sector DTC. When the load is applied visible around the midpoint of both graphs there is a noticeable increase in current amplitude. This change indicates the motor's response to the increased torque demand, confirming that the control system is functioning correctly under loaded conditions., the 12 sector DTC demonstrates better dynamic response after the load application, with a faster and more stable recovery, these experimental results validate the advantages of the 12 sector DTC, particularly in reducing torque ripple and enhancing current quality in alignment with the outcomes predicted in simulation.

a) b)

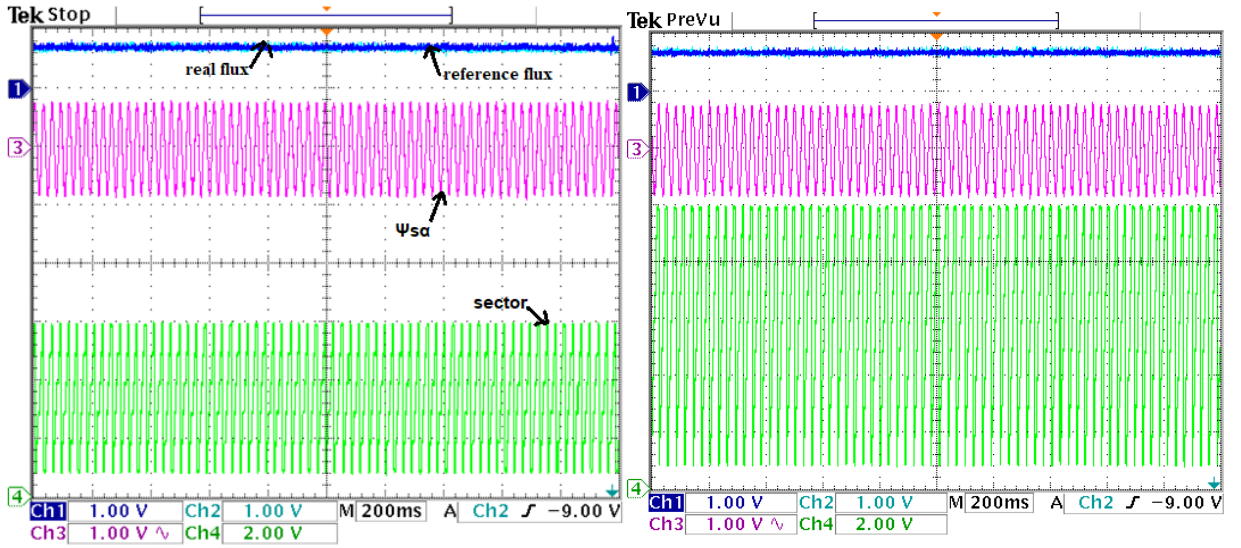

Ch1: reference flux ,Ch2:real flux,Ch3:Ψsα,Ch4:sector

Figure (4.16): the real and reference flux, Ψsα,6 and 12 sector

a) b)

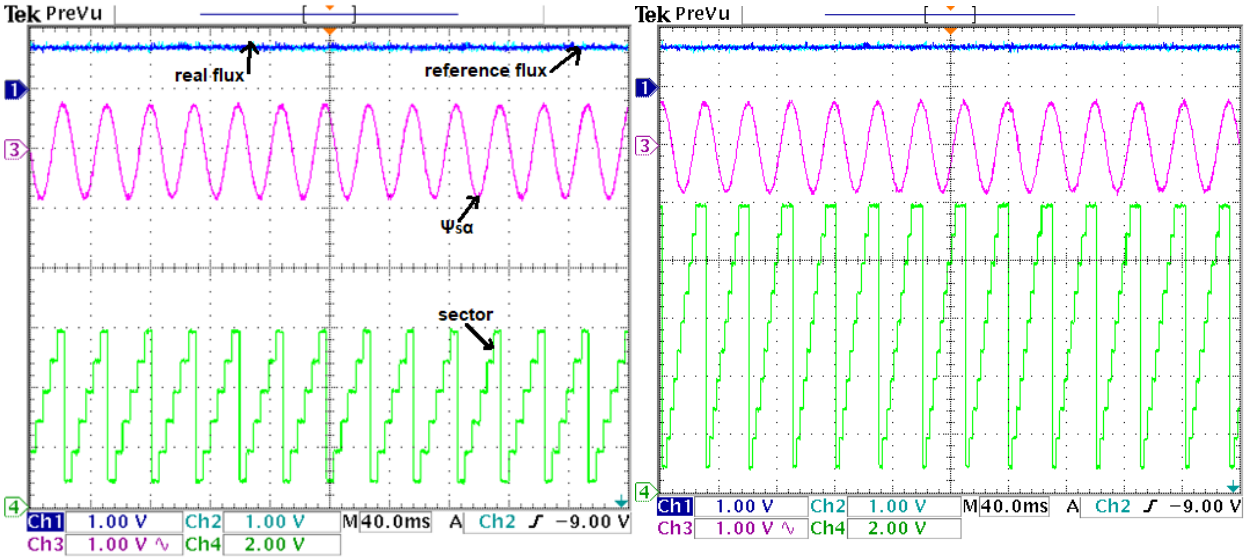

Ch1:reference flux ,Ch2:real flux,Ch3:Ψsα,Ch4:sector

Figure (4.17): ZOOM IN the real and reference flux, $\Psi_{s\alpha}$,6 and 12 sector

In both (a) and (b), the reference and real flux waveforms are displayed. In the 6 and 12 sector , the real flux (Ch2) follows the reference, The signal Ψsα (Ch3) represents the variation of the α component of the stator flux. In the 6 sector control, Ψsα has more distortion and irregular ripple but With the 12 sector control this component becomes more sinusoidal and stable.

the sector number the controller is operating in. In the 6 sector DTC (a), the transitions between sectors are more abrupt and cover wider angular intervals (60° per sector), leading to coarser control. The 12 sector DTC (b), with narrower sector widths (30° per sector), This results in better performance, as evidenced by smoother flux evolution and lower ripple.

4.10.Conclusion

Following up on the simulations, we actually put the proposed control methods to the test in this chapter using a 3 kW asynchronous motor. For this, we used the dSPACE 1104 board – it's a real workhorse for this kind of thing because it's got the processing power and accuracy to handle all sorts of complex motor controls.

Now, as anyone who's done experimental work knows, getting good data hinges on how well you can grab and process signals. You need decent sensors for that. In this chapter, we only got around to doing the experiments for the standard control methods you know, the classic DTC and the 12 sector DTC.

On a similar note, we just didn't have the resources to do the experimental work on those more advanced techniques yet, so that's something we're aiming for in the future ,The experimental results we did get? We lined them up against the simulation results from the same tests. And you know what? The theoretical stuff and the real world results were surprisingly similar. What's more, these results really showed that the control methods we were proposing actually work and are pretty accurate for controlling an asynchronous motor.

The experimental findings pretty much backed up what we saw in the simulations across all the different tests. This reinforced that the 12 sector DTC control is a step up from the regular one.

So, while the experiments in this chapter were just a few basic tests with traditional controls (again, those pesky technical issues), the plan is to dive into those smart controls and maybe even try out some other ways to control the motor's torque down the line.

Ultimately, we achieved what we set out to do in this chapter: to get those conventional control techniques up and running and validated using the dSPACE board.

General Conclusion

As part of the research on the control of asynchronous machines, our main objective was to study and practically implement the DTC control strategy.

In the first chapter, a general modeling study of the induction machine was presented, taking into account simplifying assumptions. This model clearly highlights the coupling between the electromagnetic torque and the stator flux. To achieve efficient control of the asynchronous machine inverter system, it is essential to decouple the electrical and mechanical parts , and we presented the model of the asynchronous machine in the Park reference frame, which reduces the number of equations from six to four global equations using simplifying assumptions.

In the second chapter, we first presented control techniques for the asynchronous machine, giving an overview of scalar control based on rotor flux orientation as well as vector control. We highlighted their challenges and limitations, particularly their sensitivity to changes in machine parameters.

In the third chapter, we presented the DTC control of the asynchronous machine powered by a two level inverter. In the first part, we studied the conventional DTC applied to the two-level inverter connected to the stator of the machine. In the second part, a 12 sector DTC approach was proposed as an alternative to the classical regulation method to enhance the motor's performance. Simulation results show that increasing the number of sectors helps reduce torque and stator flux ripples.

In the fourth chapter, the control techniques proposed in this work were experimentally validated using the ds PACE 1104 board. Several real-time tests were conducted to assess the robustness of the proposed strategies and determine which control method performs best for motor control. The experimental results confirm the effectiveness of the methods, showing strong performance particularly for the 12-sector DTC, which demonstrated reduced torque and stator flux ripples, better decoupling, and accurate reference tracking. These experimental findings also support and validate the simulation results.

Finaly The comparison between classical DTC (6 sectors) and the improved 12 sector DTC shows that increasing the number of sectors significantly enhances control performance by reducing torque and flux ripples and improving dynamic response. However, ripple and variable switching frequency issues still persist. Future improvements could involve integrating intelligent control methods (like fuzzy logic or neural networks), adopting fixed switching frequency techniques, or using model predictive control to achieve more precise and efficient regulation. These enhancements aim to further increase robustness, reduce losses, and optimize real-time performance for advanced motor drive applications.

Bibliographic References

[1] Abdelkarim AMMAR Amélioration des Performances de la Commande Directe de Couple (DTC) de La Machine Asynchrone par des Techniques Non-Linéaires r – Biskra, 29-Jun-2017

[2] Induction Machines: Their Types and Working Principle - Mango Engineer ogeshP.surwade

[3] aya patil dalve ,ogesh P.surwade SOUL 2.0 (Software for University Libraries) For Library Automation ,See discussions, stats, and author profiles for this publication at: https://www.researchgate.net/publication/343546075 Induction Motors: Construction, Principle of Operation, Power and Torque Calculations, Characteristics and Speed Control March 2021

[4]copyright 2024 All rights reserved 2012/2024 electrical technology https://www.electricaltechnology.org/2024/05/difference-between-squirrel-cage-wound-rotor-slip-ring.html

[5] Edith Clarke, "Circuit Analysis of AC Power Systems. Vol. I.", Wiley, New York, 1943 Kalyan Kumar, "Power System Stability and Control, Chapter 3", Indian Institute of Technology Madras, Chennai, India , 22 November 2020, at 07:51.Clarke Transform - Open Electrical

[6] OULED MOHAMED ,SALEM SIDI MOHAMED, Commande Directe du Couple(DTC) d'une Machine Asynchrone à Cage,Master, Université de Ghardaïa,2014/2015.

[7] MAAOUCHE Amer , HEDROUG Bachir, Commande vectorielle d'une machine électrique asynchrone triphasé ,LE DIPLOME DE MASTER, Université de Mohamed El-Bachir El-Ibrahimi - Bordj Bou Arrerid, 2020/2021.

[8] Texas Instrument, Bilal Akin,Manish Bhardwaj SensoredFieldOrientedControlof3-PhaseInduction Motors ApplicationReport SPRABP8–July2013

[9]See discussions, stats, and author profiles for this publication at: https://www.researchgate.net/publication/282859207 Review on Field Oriented Control of Induction Motor Article · July 2015

[10] [10] Selatni Abdellah, Rouina Bilal, Commande Vectorielle de la Machine Asynchrone a Flux Rotorique Orienté ,Master,Université de Biskra, 2021-2022

[11] Methods of Vector Control for Induction Motors L. Varga1, M. Kuczmann2 1Audi Hungaria Zrt, Department of Petrol Engines Audi Hung´ aria ´ ut 1, 9027, Gy″ or, Hungary E-mail: mail@vargalaszlo.com 2Sz´ echenyi Istv´ an University, Department of Automation Egyetem t´ er 1, 9026, Gy″ or, Hungary E-mail: kuczmann@sze.hu

[12] Sabour.K, Elazazi.S,Commande vectorielle da la machine asynchrone à double alimentation ,mémoire master, université AKLI Mohaned Oulhadj de Bouira, année 2015

[13] Cherier.F, Amade. G, Modélisation en vue du diagnostic des défauts dans une machine asynchrone, mémoire d'Ingénieur d'Etat, Université M'hamed Bougara-Boumerdès, 2009.

[14] Henry Ney, « Électro système-1ére SIT » livre, édition technique1997

[15] Claude Chevas, Grégory Valentin, Machine asynchrone, cours et problèmes, version du 21/09/2014.

[16] Theodor.W, Gilbert.S, « Electrotechnique » livre, 3émme édition, 1999.

[17] franck weinbissinger. «*L'alimentation électrique pour les moteurs asynchrones*».White paper ,07/2010

[18]Ridha ZAITER Comment la commande direct du couple dtc d'un machine asynchrone avec défaut.Magister,11/06/2013

[19] http://dspace.univ-tiaret.dz/chapitre 3.pdf Contrôle Directe de Couple (DTC) de la MAS à Cinq Phases

[20] Review of recent advancements of direct torque control in induction motor drives – a decade of progress ISSN 1755-4535 Received on 9th May 2017 Revised 3rd August 2017 Accepted on 31st August 2017 E-First on 13th November 2017 doi: 10.1049/iet-pel.2017.0252 www.ietdl.org

[21]Ahmed M. T. Ibraheem Al-Naib ,Northern Technical University, May 2019 DC Motors

[22] SAWALHA Anas, Ayman Abdelhadi, Commande DTC-prédictive d'un moteur asynchrone triphasé ,Master,Université Abderrahmane Mira De Bejaia, 2019/2020

[23]Chemini Kawther Commande DTC de la machine asynchrone : Etude théorique et expérimentale,Université Mohamed Khider de Biskra ,,Master, mardi 20 juin 2023

[24] AKKOUCHI KAMEL,Commande directe du couple (DTC) d'une machine asynchrone. MAGISTER , UNIVERSITE BADJI MOKHTAR- ANNABA ,Année 2007.

[25]Tidjani MAHNI,Etude et Conception dun Filtre Actif Parallele Triphase a Quatre Fils en vue des a Commande pardes Methodes d Intelligence Articielle, Doctorat en sciences, 19-Feb-2017

[26] ALNASIR, Z.A. ALMARHOON A.H, Design of Direct Torque Controller of Induction Motor (DTC), Alnasir, Z.A. et al. / International Journal of Engineering and Technology (IJET),April/2012.

[27] Performance Improvement of DTC for Induction Motor with 12 - Sector Methodology S.Pavithra, A.Sivaprakasam, T.Manigandan

Annex A

A.1. Experimental Setup Parameters:

- Rated power: 3 kW
- Rated load torque: 20 Nm
- Rated current: 10.9/6.30 A
- Rated voltage: 230/400 V
- Rated stator frequency: 50 Hz
- Rated rotor speed: 1430 rpm
- Number of pole pairs: 2
- Rated stator flux: 0.8 Wb
- Stator phase resistance R_s=2.3 Ω
- Rotor phase resistance R_r=1.8 Ω
- Stator phase self-inductance L_s=0.261 H
- Rotor phase self-inductance L_r=0.261 H
- Mutual inductance L_m=0.258 H
- Moment of inertia of rotating masses J=0.03 kg.m^2
- Friction coefficient *f*=0.002 Nm

Annex B

Conventional Speed Regulation

In industrial applications, regulating speed is crucial to mitigate undesirable load variations. A closed-loop control system is typically implemented using a Proportional Integral (PI) controller, which combines both proportional and integral actions. This approach enhances the system's performance in both steady-state and transient conditions (refer to Figure B.1).

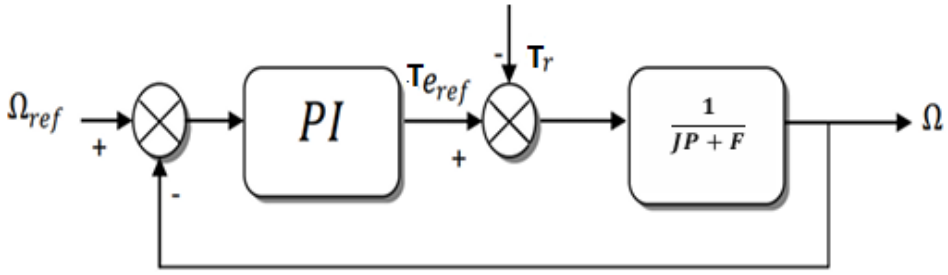

The time domain equation of this controller is given below:

$$u(t) = K_p e(t) + K_i \int_0^t e(t)dt \qquad \text{(B.1)}$$

where e(t) u(t), K_p, and K_i denote, respectively, the error at time t, the generated control signal, and the proportional and integral gains of the controller.

The corresponding transfer function is given by:

$$PI(P) = K_p + \frac{K_i}{P} = K_p\left(1 + \frac{1}{\tau P}\right) \qquad \text{(B.2)}$$

where P is the Laplace differential operator, and $\tau = K_p / K_i$ represents the time constant.
The closed loop transfer function is given by:

$$FTBF = \frac{PI(P).\frac{1}{JP+F}}{1+PI(P).\frac{1}{JP+F}} \quad \text{(B.3)}$$

By substituting equation (B.2) into equation (B.3), with $T_r = 0$ and after simplification, we obtain:

$$FTBF = \frac{(1+\tau P)}{\frac{J}{K_i}P^2+\left(\frac{F+K_p}{K_i}\right)P+1} \quad \text{(B.4)}$$

To ensure proper closed-loop control of the system, it is essential to carefully select the coefficients K_p and K_i In this case, the pole placement method is used for this selection. The transfer function of a second order closed-loop system is characterized by:

$$F(s) = \frac{K}{1+\frac{2\xi}{\omega_n}P+\frac{1}{{\omega_n}^2}P^2} \quad \text{(B.5)}$$

Thus, the characteristic equation is:

$1+\frac{2\xi}{\omega n}\omega P+\frac{1}{\omega n}P^2$

By matching it with the equation derived in expression (B.4), we obtain the following system:

$$\begin{cases} \frac{1}{{\omega_n}^2} = \frac{J}{K_i} & \Rightarrow K_i = J{\omega_n}^2 \\ \frac{2\xi}{\omega_n} = \frac{K_p+F}{K_i} & \Rightarrow K_p = \frac{2\xi K_i}{\omega_n} - F \end{cases} \quad \text{(B.6)}$$

The controller gains are selected to achieve a minimal response time while ensuring no overshoot.

This technique involves setting specific values for the damping ratio ξ and the natural frequency ω_n to determine the coefficients K_p and